

Beginner's guide to visual analysis of perovskite and organic solar cell current density-voltage characteristics

Albert These^{1,2}, L. Jan Anton Koster³, Christoph J. Brabec^{1,4}, and Vincent M. Le Corre^{*1}

¹Friedrich-Alexander-Universität Erlangen-Nürnberg (FAU), Materials for Electronics and Energy Technology (i-MEET), Martensstraße 7, 91058 Erlangen, Germany

²Friedrich-Alexander-Universität Erlangen-Nürnberg (FAU), Erlangen Graduate School in Advanced Optical Technologies (SAOT), Paul-Gordan-Str. 6, 91052 Erlangen, Germany

³Zernike Institute for Advanced Materials, University of Groningen, Nijenborgh 4, 9747 AG Groningen, The Netherlands

⁴Helmholtz-Institute Erlangen-Nürnberg (HI ERN), Immerwahrstraße 2, 91058 Erlangen, Germany

November 20, 2023

Abstract

The current density-voltage characteristic (JV) is a critical tool for understanding the behaviour of solar cells. In this article, we present an overview of the key aspects of JV analysis and introduce a user-friendly flowchart that facilitates the swift identification of the most probable limiting process in a solar cell, based mainly on the outcomes of light-intensity-dependent JV measurements. The flowchart was developed through extensive drift-diffusion simulations and a rigorous review of the literature, with a specific focus on perovskite and organic solar cells. Moreover, the flowchart proposes supplementary experiments that can be conducted to obtain a more precise prediction of the primary performance losses. It therefore serves as an optimal starting point to analyse performance losses of solar cells.

Introduction

Current density-voltage characteristic (JVs) are widely acknowledged as the cornerstone in solar cell (SC) research, since they allow for the quantification of a cell's power conversion efficiency (PCE). However, their significance goes beyond mere efficiency measurements. JVs also provide valuable qualitative insights into the working mechanisms of a SC through careful analysis of their shape and the trends observed in light-intensity-dependent JV measurements.

This guide presents a step-by-step approach to analyse SCs and identify performance-limiting factors through the analysis of JV curves. These insights are then utilized to create a flowchart that systematically identifies the primary sources of performance losses in SCs.

A typical JV curve is illustrated in Figure 1a. Three key parameters are important to consider when analysing it: the open-circuit voltage (V_{OC}), the short-circuit current density (J_{SC}) and the fill factor (FF). The open-circuit voltage is the voltage at which the net current through the cell is zero and the short-circuit current density is the current density at which the outer cell voltage is zero. The fill factor is defined as:

$$FF = \frac{J_{MPP}V_{MPP}}{J_{SC}V_{OC}}, \quad (1)$$

where J_{MPP} and V_{MPP} denote the current density and voltage at the maximum power point (MPP), respectively. Geometrically, it corresponds to the largest rectangle that fits within the JV curve and is defined by the ratio of the areas formed by $J_{SC} * V_{OC}$ and $J_{MPP} * V_{MPP}$. Ultimately, the PCE is defined by:

$$PCE = \frac{P_{out}}{P_{in}} = \frac{J_{SC}V_{OC}FF}{P_{in}}, \quad (2)$$

with P_{in} and P_{out} being the incident light power and the output electrical power, respectively.

In brief, the V_{OC} is determined by the difference in the quasi-Fermi levels of the electrons and holes in the active layer (AL) of the SC. The J_{SC} is governed by the absorption of the AL and the charge generation rate. The FF is determined by the charge extraction and transport

in the AL, transport layers (TLs) and contacts. The equivalent circuit shown in Figure 1b represents a theoretical circuit diagram of a SC and is often used to describe and model the JV. The circuit consists of a current source I_L in parallel with a diode. The parallel shunt resistance R_{SH} represents an unwanted current path that diminishes cell performance. I_L is connected to a load via a series resistance R_S . Such a SC circuit is described by the non-ideal diode equation and can be used to determine the output current I at voltage V :

$$I = -I_{ph} + I_0 \left[\exp \left(-q \frac{V - R_S I}{nk_b T} \right) - 1 \right] + \frac{V - R_S I}{R_{SH}} \quad (3)$$

Hereby, I_{ph} is the photocurrent which is generated by the incident light on the SC, I_0 is the saturation current related to recombination, q the charge, k_b the Boltzmann constant, T the temperature and n the ideality factor representing the deviation from the ideal diode behaviour.

However, such circuit modelling reveals only little insight of the physical processes governing the JV. For example, charge recombination processes are not explicitly included in the circuit model, but only implicitly through the ideality factor n . As shown in Figure 1c and described in section III one can empirically determine the ideality factor by doing light intensity dependent JV measurements, but the physical origins are not revealed.

Hereto, one has to model the charge carrier recombination explicitly. Recombination events are schematically illustrated in Figure 1d for a hypothetical SC. Charge carriers are generated in the AL and subsequently traverse through drift and diffusion mechanisms. They are then extracted by the TL and contacts or undergo recombination. In this context, recombination can occur radiatively, often involving a bimolecular process that results in photon emission. Alternatively, non-radiative recombination can take place via defect states within the bandgap, referred to as Shockley-Read-Hall (SRH) recombination. This non-radiative process may occur

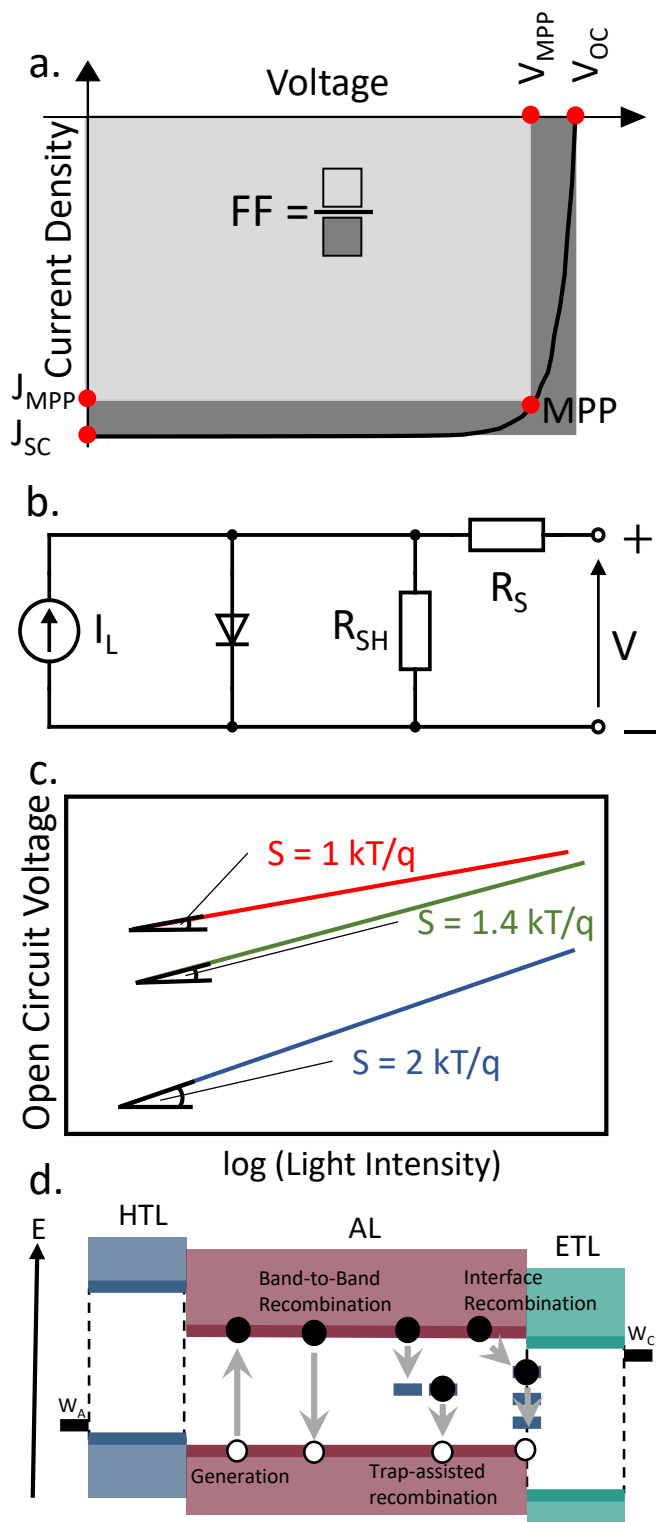


Figure 1: (a) A typical JV curve of a SC showing key parameters. (b) An equivalent circuit for a SC used to model JV curves. (c) Semi-log plot of V_{OC} as a function of light intensity: the slope of the curves can be used to estimate the ideality factor. (d) A schematic band diagram of a SC showing common recombination mechanisms

within either the AL or TL, or at the AL/TL interface. The magnitude of all these processes significantly influences the characteristics of the JV in a complex manner and necessitates modelling through drift-diffusion simulations.

The evolution and overall shape of such effects on the JV will be the foundation of the flowchart. The flowchart path is determined by answering straightforward questions at each node, leading to the endpoint that identifies the most probable cause of the performance loss. Most of the times, the questions can be answered from analysing the JVs, sometimes additional information about the device is necessary.

The decisions at each node are supported by drift-diffusion (DD) simulations as well as references to previous studies for readers wishing for a more in-depth understanding. Occasionally, additional experiments are also suggested to get to a more accurate and definitive prediction of the main losses.

The flowchart is designed to be easily understood by a reader. While it will give the right conclusion in most cases it is not excluded that some exotic situations will require a more detailed analysis. The primary focus is on the analysis of thin-film solar cells like perovskite and organic solar cells. While most of the conclusions and trends discussed here would still hold for more classical photovoltaic technologies such as silicon solar cells, there may be some discrepancies.

The flowchart was designed with the support of DD simulations using two representative sets of parameters, one for a typical organic solar cell (OSC) and the other for a perovskite solar cell (PSC). The simulation parameters can be found in supporting information (SI) Tables S1 and S2 with the corresponding fits to real experimental data (Figures S1, S2), taken from ref. 1 for PSC and 2 for OSC.

A few words about drift-diffusion simulations

Drift-diffusion simulations have been widely used to further understand the device physics of

many different solar cell technologies.^[3–6] They can be used to model the behaviour of a device in a wide range of conditions and to quantify the device’s performance parameters.

Briefly, a DD simulation is a numerical simulation that solves the Poisson and continuity equations as well as the current, drift, and diffusion of charges. Typical input parameters for DD modelling include fundamental semiconductor material properties such as energy levels, mobilities, recombination rate constants, defect/doping densities, etc.^[4–7]

The details of DD simulations are beyond the scope of this guide and can be found, for example in refs. 4,6,7. Nevertheless, we strongly advise readers to explore the literature on DD as, it can offer valuable insights that foster a critical evaluation of experimental results. Numerous papers used DD to investigate the limitations of some classical opto-electrical measurements which we also strongly recommend.^[5,6] One of the advantages DD simulations is the ability to independently investigate the impact of individual parameters, which is rarely possible through experiments alone. We will take advantage of this characteristic of DD simulations when we discuss the impact of the different parameters on the JVs at the different nodes in the flowchart. Here, all the simulations were performed using the open-source drift-diffusion package SIMSalabim.^[7,8], which has an easy to use web interface than can be accessed online.^[9] All of the simulations described in the following can also be reproduced using the Python scripts available on GitHub.^[10]

Flowchart

The flowchart is presented in Figure 2. To ensure clarity, the flowchart will be discussed from left to right and top to bottom. Each endpoint indicating a loss mechanism will be supported by a DD simulation.

The grey diamond shaped nodes represent decision nodes where a ‘yes-no’ question is posed. For clarity, the answer ‘yes’ is represented by the green line and the ‘no’ by the red lines.

The answers can be directly determined either from the JV, by knowledge about your device, or by performing the suggested experiments. The blue rectangles are process nodes that require an additional action (i.e. supplementary experiments besides JV measurements) that have to be performed before continuing to the next node.

To simplify the structure of the flowchart, we have summarized most tasks in several cases. The green rounded rectangles represent the endpoints which should give you the dominant loss. However, it is important to note that reaching an endpoint early in the tree does not necessarily exclude the losses in the subsequent branches. It is therefore useful to explore the tree further down, even if an endpoint has been reached. However, if you do not fall into one of these early endpoints then the corresponding loss mechanism can be excluded. We added the relevant section number to each process and result node in brackets to guide the reader to the corresponding paragraph in the main text and simulations in the supplementary information (SI).

In the following, we intentionally refrain from providing any numerical values to define what a good or bad range for the different figures-of-merit is, because such assessments are system dependent. The Shockley-Queisser limit^[11] provides a good baseline to estimate the loss of the different figure-of-merits. We strongly recommend readers to use online resources with tabulated values^[12] or different codes capable of calculating the Shockley-Queisser limit^[13,14] to calculate these losses.

However, one must not forget that what is considered a good value also depends a lot on the technology being studied and the reported state-of-the-art performances. For example, the best-in-class OSCs have reached FF values just below 0.82^[15], whereas record values for PSC can each values as high as 0.85.^[16]

Our analysis starts with the J_{SC} , as it is the easiest parameter to assess. As can be followed from the flowchart in Figure 2, a low J_{SC}

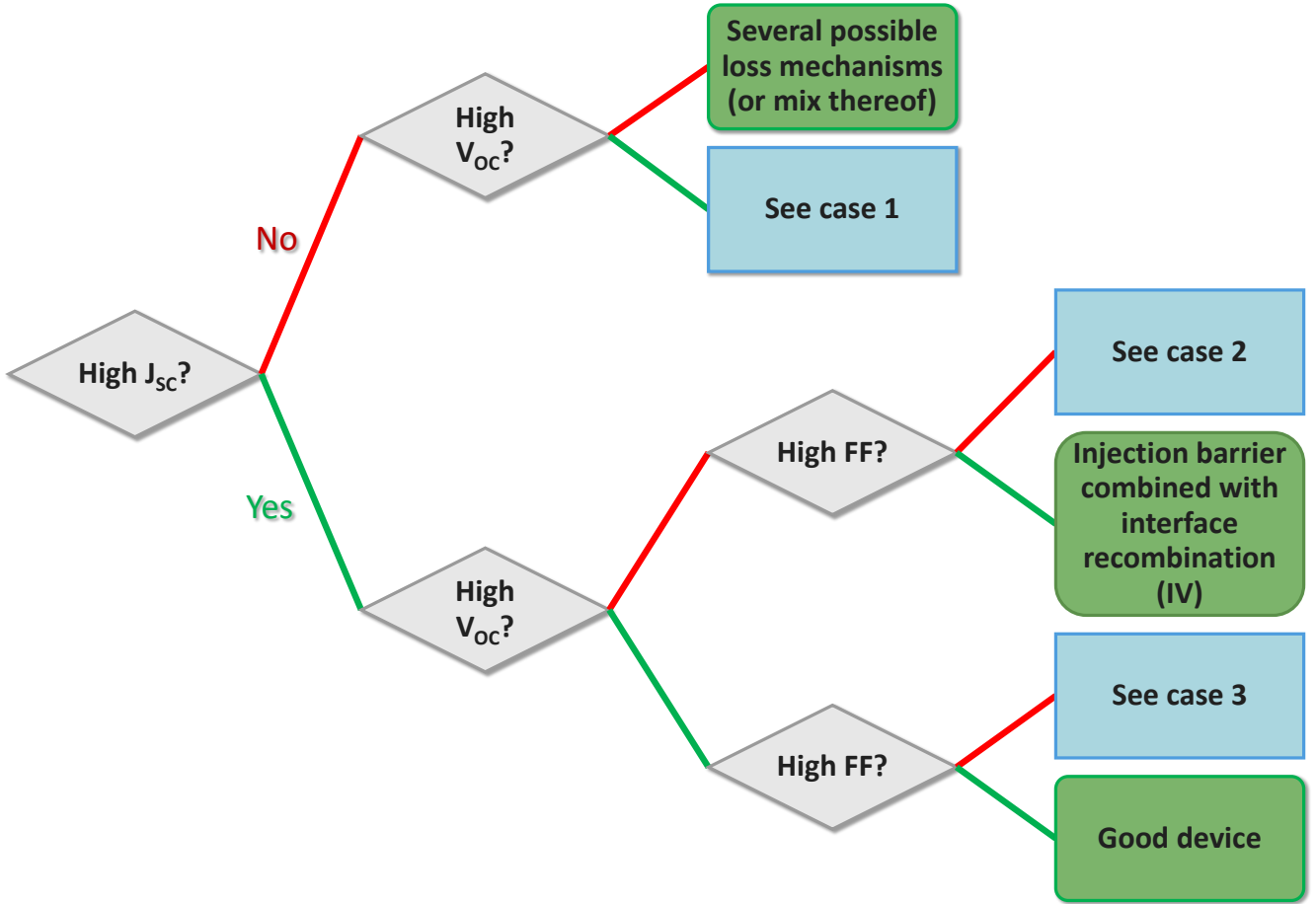


Figure 2: Flowchart to systematically analyse JV characteristics of PSC and OSC.

and V_{OC} value lead to the worst-case scenario: there are several possible loss mechanisms (or a combination thereof) affecting the cell that are impossible to entangle without additional experiments or information about the device. We discuss the origins of these losses in **Cases (1-3)** and one can check there, which loss can be excluded for the analysed device. Otherwise, if the J_{SC} is low, but the V_{OC} satisfactory, losses are generally due to the effects describes in **Case 1** (see Figure 3). First, you need to ensure that the AL creates enough photogenerated charge carriers.

(I) Charge carrier generation losses:

The main parameter that strongly affects the J_{SC} without reducing V_{OC} considerably is the AL absorption and by extension the free-charge carrier generation rate (G). Figures S3-S4 demonstrate the direct correlation between J_{SC} ,

the AL thickness (L) and the average generation rate. In most cases, i.e. in the absence of other potential losses that affect the J_{SC} and are described in the following, it can be expressed as follows:

$$J_{SC} = qGL, \quad (4)$$

with q being the electric charge.

In the event of a low J_{SC} the initial consideration is to examine is whether the AL is absorbing enough or not. The absorption of the AL can be assessed by measuring the absorption spectra, although in many cases, a visual inspection is sufficient: a transparent AL suggests that absorption might be limited. A poor absorption is most likely related to either a low absorption coefficient from the AL material itself, or to an AL that is simply too thin. Additionally, a current loss could also be attributed to parasitic absorption from the other

layers. This can be checked by performing additional absorption measurements of the other layers or by using transfer matrix modelling to assess the parasitic absorption and the expected J_{SC} from an optical standpoint. We strongly recommend readers to use SIMsalabim^[7,8] or the resources provided by the McGehee^[17,18] and Armin's^[19,20] groups if they wish to perform such simulations. Note that G and hence J_{SC} can be calculated from transfer matrix modelling and using equation 4 and, if properly corrected for the internal quantum efficiency, it can be compared to the experimental current to quantify the current loss due to non-optical processes which will be discussed later.

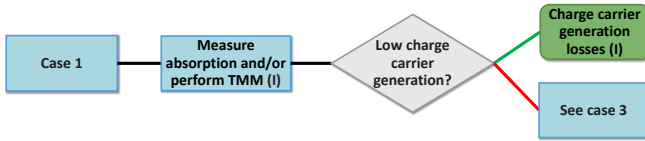


Figure 3: Flowchart illustrating the decision-making process for case 1 with low J_{SC} and high V_{OC}

If low absorption in the AL can be excluded as a reason for a low J_{SC} , we fall into **Case 3** (see Figure 5) which is addressed later. However, it should be noted that the losses described in **Case 3** need to be significant to impact the J_{SC} significantly.

We now move on to the bottom half of the tree, where the scenarios having a good J_{SC} are considered. If both the V_{OC} and FF are low then we fall into **Case 2** (see Figure 4).

(II) Shunt resistance losses:

The first and easiest loss to check when having a good J_{SC} and bad FF and V_{OC} is the shunt losses. To visually assess if shunts are a dominating factor, one needs to look at the slope at J_{SC} . If it is large (under 1 sun illumination) then shunt resistance (R_{SH}) is a likely loss. Figures S5-S6 demonstrate that examining the dark-JV at low voltages for high current densities is a good way to judge if R_{SH} is low. Plotting the light intensity dependent V_{OC} and FF is also a

useful, and often forgotten, way to check for R_{SH} losses. Typically, if both values significantly decrease at low light intensity, it indicates that shunt losses are significant. They become increasingly limiting for the performance of the cell if this plummeting regime approaches the 1 sun light intensity. One can also compare the J_{SC} in dark and under illumination. Hereby, the empirical formulas shown in equations 5 and 6 derived in the supporting information can be used to estimate the influence of shunt resistance on the V_{OC} and FF respectively (see Figures S31 and S32).

The FF is not detrimentally affected by a low R_{SH} , if the following condition is met:

$$\frac{J_{SC}}{J_{dark}(-1V)} \gtrsim 100 \quad (5)$$

Here, $J_{dark}(-1V)$ is the dark current density at -1 V (beware of the low breakdown reverse bias of PSC).

The V_{OC} is less sensitive to a leakage current and is not detrimentally affected if the following condition applies:

$$\frac{J_{SC}}{J_{dark}(-1V)} \gtrsim 5 \quad (6)$$

The shunt resistance can be quantified with different methods: (a) by taking the slope at J_{SC} with $R_{SH} = \left| \frac{1}{\text{slope}_{J_{SC}}} \right|$ (hereby, $\frac{J_{SC}}{J_{dark}(-1V)}$ can also be replaced by $J_{SC} * \text{slope}_{J_{SC}}$ in eq. 5 and 6), (b) by calculating the differential resistance^[21], or (c) by fitting of the dark-JV (or dark and light-JVs) with the non-ideal diode equation.^[22-24] The tools by Suckow et al.^[23,24] or by Holmgren et al.^[25,26] provide a good starting point for fitting the non-ideal diode equation. Note that method (a) can lead to unreliable results since the slope at J_{SC} is affected by other mechanisms (e.g. mobile ions), hence we advise readers to preferably use methods (b) and (c).

After excluding shunts as a reason for low FF and V_{OC} , it is necessary to examine recombination losses.

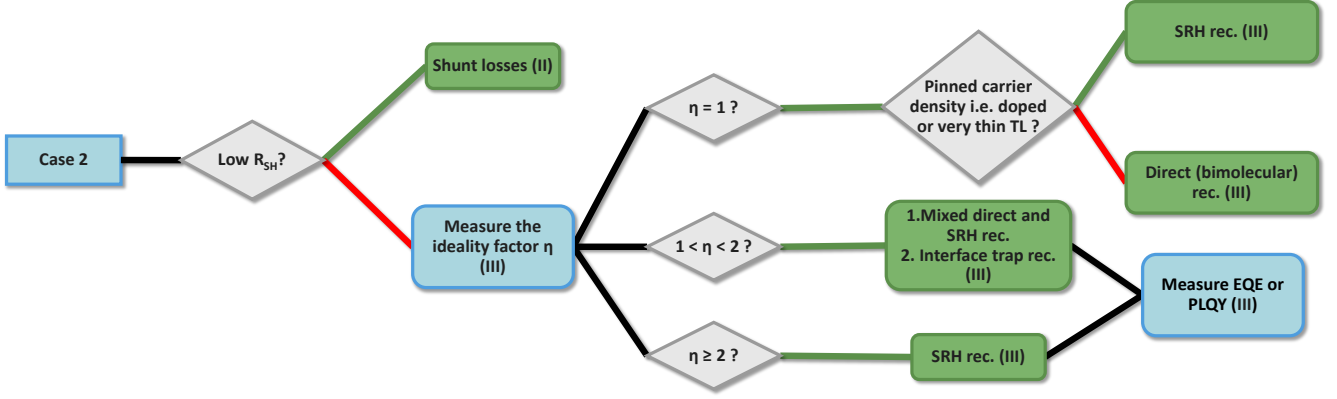


Figure 4: Flowchart illustrating the decision-making process for case 2 with high J_{SC} and low or high V_{OC} and FF .

(III) Recombination losses:

One of the easiest methods to check for recombination is to measure light-intensity dependent JVs. As shown in Figure 1c, by plotting the V_{OC} against the logarithm of the light-intensity and performing a linear fit, we can estimate the slope s which depends on the ideality factor η such that:

$$s = \eta \frac{k_B T}{q}, \quad (7)$$

with k_B being the Boltzmann constant and T the temperature.

The most common analysis of the ideality factor limits itself to suggesting that if η is close to 1 then band-to-band/bimolecular recombination is the dominant recombination process, which is however not always true. For example, the pinning of one of the carrier densities at the AL/TL interface can lead to dominant SRH recombination with an ideality factor close to 1. The charge carrier density can for example be pinned to the doping level of the TL in case of a defect rich interface and highly doped TL. If the TL is very thin, the charge carrier density can also be pinned to the energy level of the electrode, as it induces plenty of charges in the TL^[27] These effects are shown in Figures S7-S8 and S13-S14. In the absence of Fermi level pinning, the recombination is bimolecular, see Figures S9 and S15. For PSC, this recombination is radiative and directly correlated to the absorption coefficient as per detailed

balance limit^[11]. It thus will not reduce the performance of the solar cell. However, in our DD simulation, the bimolecular recombination factor is not directly connect to absorption leading to the observed trends. On the other hand, OSCs have processes that result in non-radiative second order recombination^[28] resulting in the trends shown in S15. An η between 1 and 2 is an indication for either SRH recombination or dominant recombination via interface traps (S10-S12 and S16-S18). Lastly, η can also be larger than 2 for PSC, which indicates dominant SRH recombination, see Figure S10. However, as discussed in more detail in refs. 27,29,30 other factors can also influence the ideality factor. Readers need to be careful when drawing strong conclusions from the ideality factor alone.

Ideally, we recommend performing additional experiments to confirm the conclusion drawn from analysing the ideality factor alone. For example, intensity-dependent and/or ultra-sensitive external quantum efficiency (EQE) measurements can be a good way to assess the presence of traps in the systems.^[31,32] Measuring quasi-fermi level splitting (QFLS) on the AL material, half-cells with the TLs and the AL and complete cells is also a very powerful way to pinpoint where the dominant recombination happens.^[33,34] However, depending on the technologies, different methods need to be used to measure the QFLS. For PSCs absolute

photoluminescence (PL) and quantum yield measurements are routinely used since the PL mostly depends on the recombination of free carriers.^[35,36] For OSCs, alternative methods, such as photoinduced absorption spectroscopy are suitable.^[37] In fact, the presence of exciton and charge-transfer states in organic materials and blends strongly influence the PL making it an unsuitable method to estimate the QFLS. For more insights into PL and QFLS measurements we recommend reading refs. 35–41.

(IV) Injection barrier and trapping at the transport layer to active layer interface losses:

The next endpoint occurs when one observes a high J_{SC} combined with a low V_{OC} and a relatively high FF . This is a typical signature of an injection barrier from the TL to the AL combined with significant SRH recombination occurring at that interface. Figures S20-S21 a-b demonstrate this phenomena. It can be investigated by comparing the QFLS and the V_{OC} . If they do not match, it indicates the existence of a significant injection barrier and interface recombination. This mismatch occurs due to a pinning of the QFLS at the interface which limits the V_{OC} . The papers by Phuong^[37] and Stolterfoht^[39] describe in detail how to conduct these measurements for OSC and PSC respectively.

Even in the absence of dominant traps, the presence of an injection barrier can hinder efficient charge transfer and extraction, leading to a reduction of FF as shown in S20 and S21 c-d.^[34]

However, this is only happens if the injected charge carrier mobility is low in the AL. Otherwise, an injection barrier does not affect the SC detrimentally (S20 e-f). The instances of injection barriers in absence of SRH recombination do not reduce the V_{OC} and thus are treated under **Case 3**.

If both the J_{SC} and V_{OC} are high, but the FF is low then we fall into **Case 3**.

(V) Ionic losses:

The first loss mechanism to consider in **Case 3** are ionic losses. As demonstrated in Figure S22 a-b, the presence of a high concentration of both positively and negatively charged mobile ions significantly affects the FF of PSCs, while retaining a high J_{SC} and V_{OC} . However, if the TLs are non-blocking and ions move inside the TLs, these effects are strongly mitigated and the mobile ions influence the JV less S22 c-d. Note that these mobile ions may then induce detrimental effects on long-term stability and degrade both the TLs and electrodes which affects the performance of the device over time^[42,43].

If only one polarity type is dominant, mobile ions can also lead to a low FF (Figure S23 a-b) or to a low J_{SC} (Figure S23 c-d). Non-blocking TLs again reduce the influence of both effects (not shown here). Thiesbrummel et al.,^[44] demonstrated that the ions decrease the J_{SC} by reducing the charge extraction efficiency caused by the ionic accumulation at the interface between the perovskite and TL and flattening of the bands under stabilized short-circuit condition. To assess whether ionic losses are significant, one needs to perform either fast hysteresis measurements as described in ref. 1 or measure the transient current decay as described in ref. 44.

If ionic losses can be excluded then one has to examine the slope at J_{SC} . If it is high, we have to ensure that we do not have any shunt losses, as already described in section II.

(VI) Field-dependent charge carrier generation losses:

Another common phenomena that can lead to a high slope at J_{SC} for OSC includes field-dependant charge carrier generation.^[45] Small highest occupied molecular orbital to lowest unoccupied molecular orbital energetic offsets can lead to inefficient dissociation of excitons into charge transfer states. The dissociation is then field dependent and can lead to a reduction of the J_{SC} and FF , see Figure S24.^[46,47] To properly investigate if this process is causing

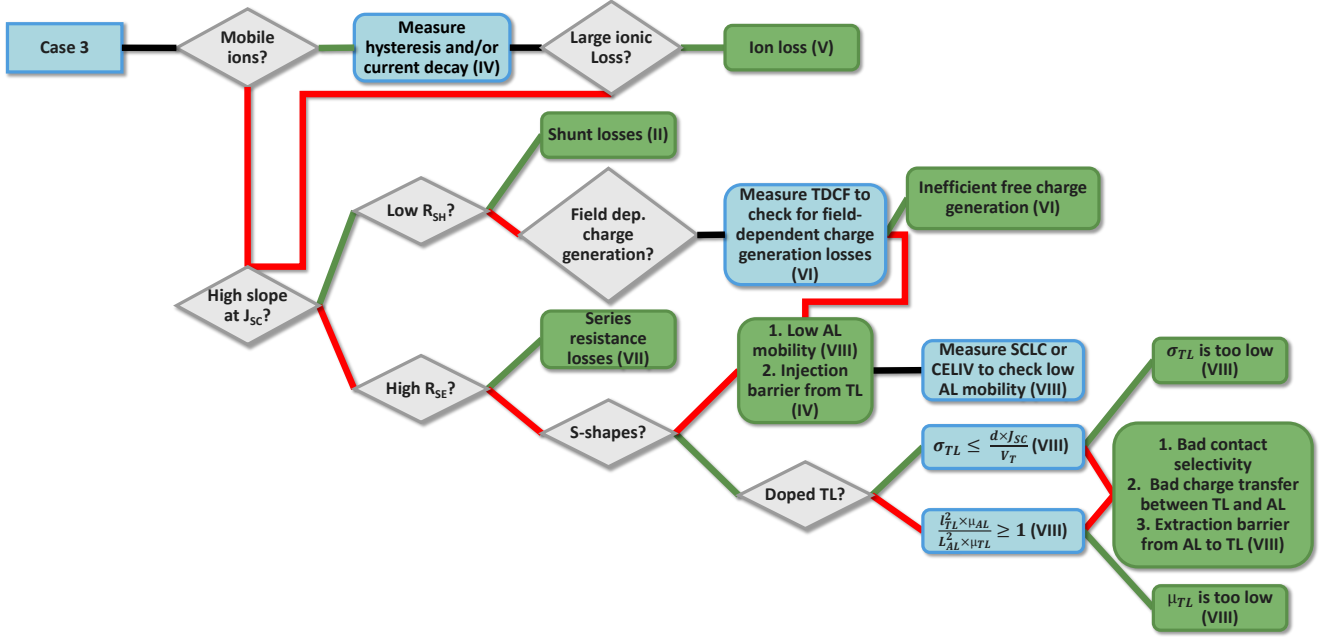


Figure 5: Flowchart illustrating the decision-making process for case 3 with high J_{SC} and V_{OC} and low FF .

the slope at J_{SC} , one needs to perform more advanced experimental techniques such as time-delayed collection field (TDCF)^[45] and/or light-intensity and voltage dependent EQE.^[48] If field-dependant charge carrier generation is not an issue, then the AL mobility is likely the limiting factor, as discussed in section VIII.

(VII) Series resistance losses:

Otherwise, if the slope is small, series resistance losses need to be examined. Similarly to the shunt resistance, the series resistance can be estimated with different methods: (a) by taking the slope at V_{OC} with $R_S = |\frac{1}{slope_{OC}}|$, (b) by calculating the differential resistance^[21] or (c) by fitting of the dark-JV (or dark and light-JVs) with the non-ideal diode equation.^[22–24,49]

Assessing the FF vs logarithm of the light intensity is good to determine if R_S strongly affects the performance at 1 sun, see Figures S25-S26. At high light intensities the FF typically decays due to R_S , as also shown in Figure S31a. If that decay starts before 1 sun then the device likely suffers from strong series resistance losses.

(VIII) Extraction and transport losses:

If all resistive issues can be excluded, the next step is to check for S-shapes. A JV-curve is said to have an S-shape, if it has an inflection point, see i.e. Figures S28 and S30. In the absence of S-shapes low electron and hole mobilities in the AL are probably responsible for the low FF , as illustrated in Figures S27 and S29. Note that for a given mobility, the AL thickness could also be too large, since the mobility-thickness ratio is the governing parameter here. To check for low AL mobility, one can calculate the effective mobility using the charge extraction by linearly increasing voltage (CELIV) measurement^[50,51]. Although it does not provide separate values for electron and hole mobilities independently, it still offers valuable information on the charge transport within the device. Another option is to perform space-charge-limited current (SCLC) measurements in a single-carrier device configuration. SCLC measurements are powerful as we can measure the electron and hole mobilities (and trap densities) separately. However, it requires the preparation of additional devices with a different device structure, which would entail further optimisation to assure comparability of

the deposited materials. In addition, making reliable SCLC measurements and extracting the correct values from this method is not always simple, we suggest readers to read refs. 52–56 for more information about SCLC.

An injection barrier from the TL to the AL can also lead to a FF loss without significant J_{SC} or V_{OC} losses, as already shown in Figure S20-S21a-b. However, this only happens if there is no strong SRH recombination at that interface as describes in section IV.

Finally, S-shapes usually appear due to an unbalanced extraction of charge carriers. Such a phenomenon can have several origins such as (a) poor TL mobility or (b) conductivity, (c) poor charge carrier transfer between the AL and the TLs, (d) injection or (e) extraction barriers from the AL to the TLs. One of the current authors previously described how to optimize the TL thickness, mobility and/or conductivity to avoid such losses and define the two figures-of-merit that appear in the flowchart.^[57]

Finally, if the J_{SC} , V_{OC} and FF are all high, one has a well performing solar cell.

Conclusion

We have presented a list of the most common loss mechanisms in PSC and OSC and showed, using DD simulations, how they affect JVs. We think that the results of this study will be useful for individuals new to the field of thin film SCs. We aim to provide beginners with a framework to visually assess and understand performance losses of solar cells only by looking at JV characteristics. Additionally, a series of references with useful resources and with more in-depth analysis of the different mechanisms is provided here. Readers are encouraged to make use of the many open-source simulation tools available online to deepen their understanding of the different mechanisms and to improve their analysis of experimental data.

Finally, it is important to emphasize that the flowchart presented here is only made for a

qualitative assessment of the dominant losses and is by no means quantitative. Nevertheless, it is a valuable starting point for the analysis of experimental data. It provides guidance on the experiment to perform next in order to obtain a definitive answer and/or quantify the main loss process. By following the suggested path in the flowchart, researchers can systematically investigate and understand the underlying mechanisms that contribute to performance limitations in their solar cells.

Acknowledgements

The authors would like to express their gratitude to S. Kahmann for the valuable feedback provided. A.T. gratefully acknowledges funding of the Erlangen Graduate School in Advanced Optical Technologies (SAOT) by the Bavarian State Ministry for Science and Art.

References

- [1] V. M. Le Corre, J. Diekmann, F. Peña-Camargo, J. Thiesbrummel, N. Tokmoldin, E. Gutierrez-Partida, K. P. Peters, L. Perdigón-Toro, M. H. Futscher, F. Lang, J. Warby, H. J. Snaith, D. Neher and M. Stollerfoht, Quantification of Efficiency Losses Due to Mobile Ions in Perovskite Solar Cells via Fast Hysteresis Measurements, *Solar RRL*, 2022, 6, 2100772.
- [2] D. Hu, Q. Yang, H. Chen, F. Wobben, V. M. L. Corre, R. Singh, T. Liu, R. Ma, H. Tang, L. J. A. Koster, T. Duan, H. Yan, Z. Kan, Z. Xiao and S. Lu, 15.34% efficiency all-small-molecule organic solar cells with an improved fill factor enabled by a fullerene additive, *Energy & Environmental Science*, 2020, 13, 2134–2141.
- [3] T. S. Sherkar, C. Momblona, L. Gil-Escrig, J. Ávila, M. Sessolo, H. J. Bolink and

- L. J. A. Koster, Recombination in Perovskite Solar Cells: Significance of Grain Boundaries, Interface Traps, and Defect Ions, *ACS Energy Letters*, 2017, 2, 1214–1222.
- [4] L. J. Koster, E. C. Smits, V. D. Mihailetschi and P. W. Blom, Device model for the operation of polymer/fullerene bulk heterojunction solar cells, *Physical Review B - Condensed Matter and Materials Physics*, 2005, 72, 1–9.
- [5] M. T. Neukom, A. Schiller, S. Züfle, E. Knapp, J. Ávila, D. Pérez-Del-Rey, C. Dreessen, K. P. Zanoni, M. Sessolo, H. J. Bolink and B. Ruhstaller, Consistent Device Simulation Model Describing Perovskite Solar Cells in Steady-State, Transient, and Frequency Domain, *ACS Applied Materials and Interfaces*, 2019, 11, 23320–23328.
- [6] M. Neukom, S. Züfle, S. Jenatsch and B. Ruhstaller, Opto-electronic characterization of third-generation solar cells, *Science and Technology of Advanced Materials*, 2018, 19, 291–316.
- [7] M. Koopmans, V. M. Le Corre and L. A. Koster, SIMsalabim: An open-source drift-diffusion simulator for semiconductor devices, *Journal of Open Source Software*, 2022, 7, 3727.
- [8] *kostergroup/SIMsalabim: A 1D drift-diffusion simulator for semiconductor devices (LEDs, solar cells, diodes, organics, perovskites)*, <https://github.com/kostergroup/SIMsalabim>.
- [9] *SIMsalabim GUI*, <http://simsalabim-online.com/>.
- [10] *JV beginner's guide repository*, https://github.com/VMLC-PV/JV_beginner_guide.
- [11] W. Shockley and H. J. Queisser, Detailed Balance Limit of Efficiency of p-n Junction Solar Cells, *Journal of Applied Physics*, 1961, 32, 510.
- [12] S. Rühle, Tabulated values of the Shockley–Queisser limit for single junction solar cells, *Solar Energy*, 2016, 130, 139–147.
- [13] M. Chuang, *marcus-cmc/Shockley-Queisser-limit: Calculation and visualization tools for theoretical solar cell efficiencies based on the Shockley Queisser limit with options to change temperature, light intensity, and radiative efficiency*, <https://github.com/marcus-cmc/Shockley-Queisser-limit>.
- [14] S. Hamady, *sidihamady/Shockley-Queisser: Shockley-Queisser limit Calculator. The Shockley-Queisser limit is the maximum photovoltaic efficiency obtained for a solar cell with respect to the absorber bandgap*, <https://github.com/sidihamady/Shockley-Queisser>.
- [15] X. Zhang, C. Li, J. Xu, R. Wang, J. Song, H. Zhang, Y. Li, Y. N. Jing, S. Li, G. Wu, J. Zhou, X. Li, Y. Zhang, X. Li, J. Zhang, C. Zhang, H. Zhou, Y. Sun and Y. Zhang, High fill factor organic solar cells with increased dielectric constant and molecular packing density, *Joule*, 2022, 6, 444–457.
- [16] J. Shi, F. Li, C. Liu, X. Ling, X. Zhang, Y. Wang, J. Guo, C. Zhao, D. Wang, Y. Li, W. Ma, J. Yuan and B. Xu, Inverted Perovskite Solar Cells with >85 % Fill Factor via Sequential Interfacial Engineering, *Solar RRL*, 2023, 2300078, 1–9.
- [17] G. F. Burkhard, E. T. Hoke and M. D. McGehee, Accounting for Interference, Scattering, and Electrode Absorption to Make Accurate Internal Quantum Efficiency Measurements in Organic and Other Thin Solar Cells, *Advanced Materials*, 2010, 22, 3293–3297.

- [18] *erichoke/Stanford: Scripts for Photovoltaics Research with McGehee Group*, <https://github.com/erichoke/Stanford>.
- [19] R. Kerremans, C. Kaiser, W. Li, N. Zarrabi, P. Meredith and A. Armin, The Optical Constants of Solution-Processed Semiconductors—New Challenges with Perovskites and Non-Fullerene Acceptors, *Advanced Optical Materials*, 2020, 8, 2000319.
- [20] *RobinKerremans/NKFinder: Matlab software to derive optical constants from Transmission data*, <https://github.com/RobinKerremans/NKFinder>.
- [21] V. V. Brus, C. M. Proctor, N. A. Ran, T.-Q. Nguyen, V. V. Brus, C. M. Proctor, N. A. Ran and T.-Q. Nguyen, Capacitance Spectroscopy for Quantifying Recombination Losses in Nonfullerene Small-Molecule Bulk Heterojunction Solar Cells, *Advanced Energy Materials*, 2016, 6, 1502250.
- [22] A. Jain and A. Kapoor, Exact analytical solutions of the parameters of real solar cells using Lambert W-function, *Solar Energy Materials and Solar Cells*, 2004, 81, 269–277.
- [23] S. Suckow, T. M. Pletzer and H. Kurz, Fast and reliable calculation of the two-diode model without simplifications, *Progress in Photovoltaics: Research and Applications*, 2014, 22, 494–501.
- [24] S. Stephan, *2/3-Diode Fit*, 2014, <https://nanohub.org/resources/14300>.
- [25] W. F. Holmgren, C. W. Hansen and M. A. Mikofski, pvlib python: a python package for modeling solar energy systems, *Journal of Open Source Software*, 2018, 3, 884.
- [26] *pvlib/pvlib-python: A set of documented functions for simulating the performance of photovoltaic energy systems.*, <https://github.com/pvlib/pvlib-python>.
- [27] V. M. Le Corre, T. S. Sherkar, M. Koopmans and L. J. A. Koster, Identification of the dominant recombination process for perovskite solar cells based on machine learning, *Cell Reports Physical Science*, 2021, 2, 100346.
- [28] K. Tvingstedt and C. Deibel, Temperature Dependence of Ideality Factors in Organic Solar Cells and the Relation to Radiative Efficiency, *Advanced Energy Materials*, 2016, 6, 1502230.
- [29] W. Tress, M. Yavari, K. Domanski, P. Yadav, B. Niesen, J. P. C. Baena, A. Hagfeldt and M. Graetzel, Interpretation and evolution of open-circuit voltage, recombination, ideality factor and subgap defect states during reversible light-soaking and irreversible degradation of perovskite solar cells, *Energy & Environmental Science*, 2018, 11, 151–165.
- [30] P. Caprioglio, C. M. Wolff, O. J. Sandberg, A. Armin, B. Rech, S. Albrecht, D. Neher and M. Stollerfoht, On the Origin of the Ideality Factor in Perovskite Solar Cells, *Advanced Energy Materials*, 2020, 10, 2000502.
- [31] N. Zarrabi, O. J. Sandberg, S. Zeiske, W. Li, D. B. Riley, P. Meredith and A. Armin, Charge-generating mid-gap trap states define the thermodynamic limit of organic photovoltaic devices, *Nature Communications 2020 11:1*, 2020, 11, 1–10.
- [32] S. Zeiske, O. J. Sandberg, N. Zarrabi, W. Li, P. Meredith and A. Armin, Direct observation of trap-assisted recombination in organic photovoltaic devices, *Nature Communications 2021 12:1*, 2021, 12, 1–7.
- [33] L. Q. Phuong, S. M. Hosseini, O. J. Sandberg, Y. Zou, H. Y. Woo, D. Neher and S. Shoaee, Quantifying Quasi-Fermi Level Splitting and Open-Circuit Voltage Losses in Highly Efficient Nonfullerene Organic Solar Cells, *Solar RRL*, 2021, 5, 1–6.

- [34] M. Stolterfoht, P. Caprioglio, C. M. Wolff, J. A. Márquez, J. Nordmann, S. Zhang, D. Rothhardt, U. Hörmann, Y. Amir, A. Redinger, L. Kegelmann, F. Zu, S. Albrecht, N. Koch, T. Kirchartz, M. Saliba, T. Unold and D. Neher, The impact of energy alignment and interfacial recombination on the internal and external open-circuit voltage of perovskite solar cells, *Energy and Environmental Science*, 2019, 12, 2778–2788.
- [35] M. Stolterfoht, C. M. Wolff, J. A. Márquez, S. Zhang, C. J. Hages, D. Rothhardt, S. Albrecht, P. L. Burn, P. Meredith, T. Unold and D. Neher, Visualization and suppression of interfacial recombination for high-efficiency large-area pin perovskite solar cells, *Nature Energy*, 2018, 3, 847–854.
- [36] T. Kirchartz, J. A. Márquez, M. Stolterfoht and T. Unold, Photoluminescence-Based Characterization of Halide Perovskites for Photovoltaics, *Advanced Energy Materials*, 2020, 1904134, 1904134.
- [37] L. Q. Phuong, S. M. Hosseini, O. J. Sandberg, Y. Zou, H. Y. Woo, D. Neher and S. Shoaee, Quantifying Quasi-Fermi Level Splitting and Open-Circuit Voltage Losses in Highly Efficient Nonfullerene Organic Solar Cells, *Solar RRL*, 2021, 5, 2000649.
- [38] L. Krückemeier, B. Krogmeier, Z. Liu, U. Rau and T. Kirchartz, Understanding Transient Photoluminescence in Halide Perovskite Layer Stacks and Solar Cells, *Advanced Energy Materials*, 2021, 11, 2003489.
- [39] M. Stolterfoht, P. Caprioglio, C. M. Wolff, J. A. Márquez, J. Nordmann, S. Zhang, D. Rothhardt, U. Hörmann, Y. Amir, A. Redinger, L. Kegelmann, F. Zu, S. Albrecht, N. Koch, T. Kirchartz, M. Saliba, T. Unold and D. Neher, The impact of energy alignment and interfacial recombination on the internal and external open-circuit voltage of perovskite solar cells, *Energy & Environmental Science*, 2019, 12, 2778–2788.
- [40] M. Stolterfoht, V. M. Le Corre, M. Feuerstein, P. Caprioglio, L. J. A. Koster and D. Neher, Voltage-Dependent Photoluminescence and How It Correlates with the Fill Factor and Open-Circuit Voltage in Perovskite Solar Cells, *ACS Energy Letters*, 2019, 4, 2887–2892.
- [41] C. M. Wolff, P. Caprioglio, M. Stolterfoht, D. Neher, C. M. Wolff, P. Caprioglio, M. Stolterfoht and D. Neher, Nonradiative Recombination in Perovskite Solar Cells: The Role of Interfaces, *Advanced Materials*, 2019, 31, 1902762.
- [42] R. A. Kerner, P. Schulz, J. A. Christians, S. P. Dunfield, B. Dou, L. Zhao, G. Teeter, J. J. Berry and B. P. Rand, Reactions at noble metal contacts with methylammonium lead triiodide perovskites: Role of underpotential deposition and electrochemistry, *APL Materials*, 2019, 7, 041103.
- [43] S. Bitton and N. Tessler, Perovskite ionics - elucidating degradation mechanisms in perovskite solar cells via device modelling and iodine chemistry, *Energy and Environmental Science*, 2023, 2621–2628.
- [44] J. Thiesbrummel, V. M. Le Corre, F. Peña-Camargo, L. Perdigón-Toro, F. Lang, F. Yang, M. Grischek, E. Gutierrez-Partida, J. Warby, M. D. Farrar, S. Mahesh, P. Caprioglio, S. Albrecht, D. Neher, H. J. Snaith and M. Stolterfoht, Universal Current Losses in Perovskite Solar Cells Due to Mobile Ions, *Advanced Energy Materials*, 2021, 11, 2101447.
- [45] J. Kurpiers, T. Ferron, S. Roland, M. Jakoby, T. Thiede, F. Jaiser, S. Albrecht, S. Janietz, B. A. Collins, I. A. Howard and D. Neher, Probing the pathways of free charge generation in or-

- ganic bulk heterojunction solar cells, *Nature Communications*, 2018, 9, 2038.
- [46] M. Pranav, T. Hultsch, A. Musiienko, B. Sun, A. Shukla, F. Jaiser, S. Shoaee and D. Neher, Anticorrelated Photoluminescence and Free Charge Generation Proves Field-Assisted Exciton Dissociation in Low-Offset PM6:Y5 Organic Solar Cells, 2023.
- [47] N. Tokmoldin, B. Sun, F. Moruzzi, A. Patterson, O. Alqahtani, R. Wang, B. A. Collins, I. McCulloch, L. L uer, C. J. Brabec, D. Neher and S. Shoaee, Elucidating How Low Energy Offset Matters to Performance of Nonfullerene Acceptor-Based Solar Cells, *ACS Energy Letters*, 2023, 2552–2560.
- [48] U. W urfel, L. Perdig on-Toro, J. Kurpiers, C. M. Wolff, P. Caprioglio, J. J. Rech, J. Zhu, X. Zhan, W. You, S. Shoaee, D. Neher and M. Stolterfoht, Recombination between Photogenerated and Electrode-Induced Charges Dominates the Fill Factor Losses in Optimized Organic Solar Cells, *Journal of Physical Chemistry Letters*, 2019, 10, 3473–3480.
- [49] *VMLC-PV/PVLC_Diode_Fit: Fitting non-ideal diode equation to JV-curve Transmission data*, https://github.com/VMLC-PV/PVLC_Diode_Fit.
- [50] M. T. Neukom, N. A. Reinke and B. R ustaller, Charge extraction with linearly increasing voltage: A numerical model for parameter extraction, *Solar Energy*, 2011, 85, 1250–1256.
- [51] O. J. Sandberg and M. Nyman, Charge extraction by a linearly increasing voltage of photo-generated carriers: The influence of two mobile carrier types, bimolecular recombination, and series resistance, *Organic Electronics*, 2019, 64, 97–103.
- [52] J. C. Blakesley, F. A. Castro, W. Kylberg, G. F. A. A. Dibb, C. Arantes, R. R. Valaski, M. Cremona, J. S. J. S. J.-S. Kim and J. S. J. S. J.-S. Kim, Towards reliable charge-mobility benchmark measurements for organic semiconductors, *Organic Electronics*, 2014, 15, 1263–1272.
- [53] J. A. R ohr, D. Moia, S. A. Haque, T. Kirchartz and J. Nelson, Exploring the validity and limitations of the Mott-Gurney law for charge-carrier mobility determination of semiconducting thin-films, *Journal of Physics Condensed Matter*, 2018, 30, 105901.
- [54] J. A. R ohr, Direct Determination of Built-in Voltages in Asymmetric Single-Carrier Devices, *Physical Review Applied*, 2019, 11, 54079.
- [55] E. A. Duijnste, J. M. Ball, V. M. Le Corre, L. J. A. Koster, H. J. Snaith and J. Lim, Toward Understanding Space-Charge Limited Current Measurements on Metal Halide Perovskites, *ACS Energy Letters*, 2020, 376–384.
- [56] V. M. Le Corre, E. A. Duijnste, O. E. Tambouli, J. M. Ball, H. J. Snaith, J. Lim and L. J. A. Koster, Revealing Charge Carrier Mobility and Defect Densities in Metal Halide Perovskites via Space-Charge-Limited Current Measurements, *ACS Energy Letters*, 2021, 6, 1087–1094.
- [57] V. M. Le Corre, M. Stolterfoht, L. Perdig on Toro, M. Feuerstein, C. Wolff, L. Gil-Escrig, H. J. Bolink, D. Neher and L. J. A. Koster, Charge Transport Layers Limiting the Efficiency of Perovskite Solar Cells: How To Optimize Conductivity, Doping, and Thickness, *ACS Applied Energy Materials*, 2019, 2, 6280–6287.

Supporting Information for Beginner's guide to visual analysis of perovskite and organic solar cell current density-voltage characteristics

Albert These^{1,2}, L. Jan Anton Koster³, Christoph J. Brabec^{1,4}, and Vincent M. Le Corre^{*1}

¹Friedrich-Alexander-Universität Erlangen-Nürnberg (FAU), Materials for Electronics and Energy Technology (i-MEET), Martensstraße 7, 91058 Erlangen, Germany

²Friedrich-Alexander-Universität Erlangen-Nürnberg (FAU), Erlangen Graduate School in Advanced Optical Technologies (SAOT), Paul-Gordan-Str. 6, 91052 Erlangen, Germany

³Zernike Institute for Advanced Materials, University of Groningen, Nijenborgh 4, 9747 AG Groningen, The Netherlands

⁴Helmholtz-Institute Erlangen-Nürnberg (HI ERN), Immerwahrstraße 2, 91058 Erlangen, Germany

November 20, 2023

*vincent.le.corre@fau.de

Solar cell base cases:

The base case scenario for perovskite solar cells (PSCs) was taken from ref. [?] and fitted with SIMsalabim. [? ?]

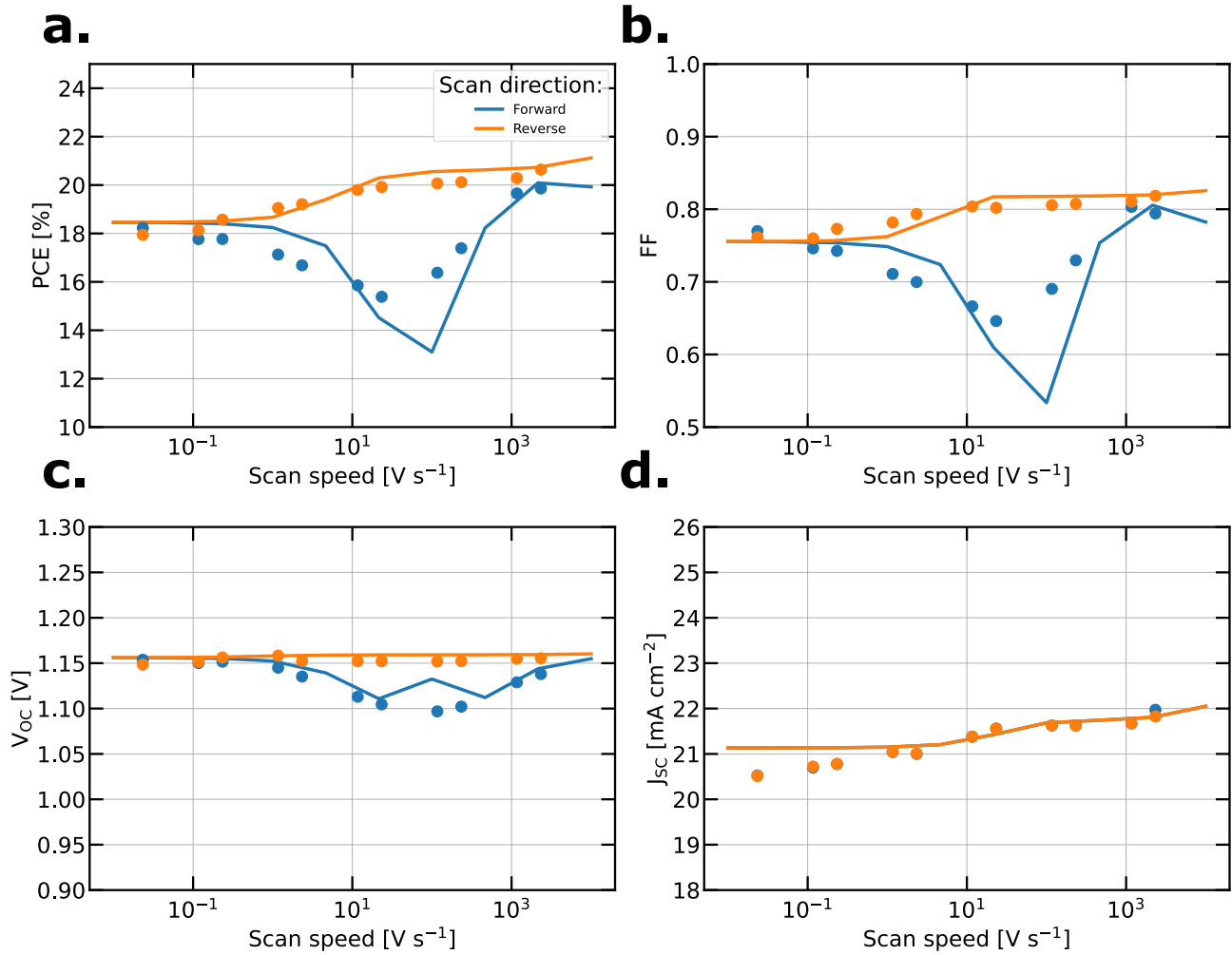


Figure S1: Performances characteristics for the base case scenario for a typical PSC with experimental data (symbols) and the corresponding fitted simulation data (lines). The PCE (a), FF (b), V_{oc} and J_{sc} are plotted as a function of bias scan speed.

The base case scenario for organic solar cells (OSCs) was taken from ref. [?] and fitted with SIMsalabim. [? ?]

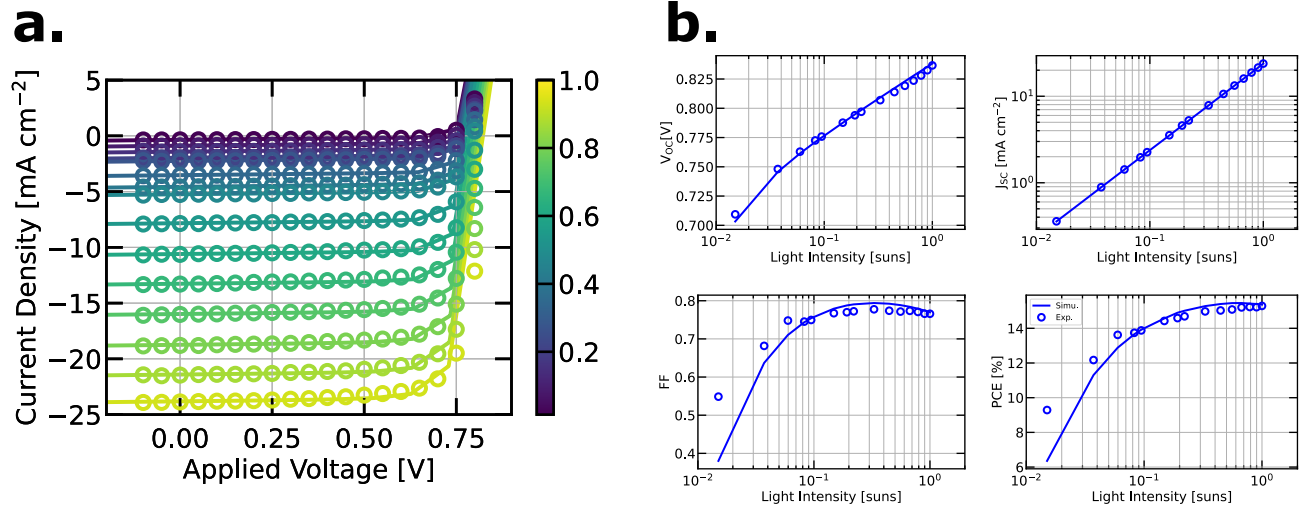


Figure S2: JVs and performances for the base case scenario for a typical OSC with experimental data (symbols) and the corresponding fitted simulation data (lines). (a) light intensity dependent JV. The colourmap indicates the illumination intensity in fractions of 1 sun. (b) light intensity dependent performances

I Charge carrier generation losses:

PSC:

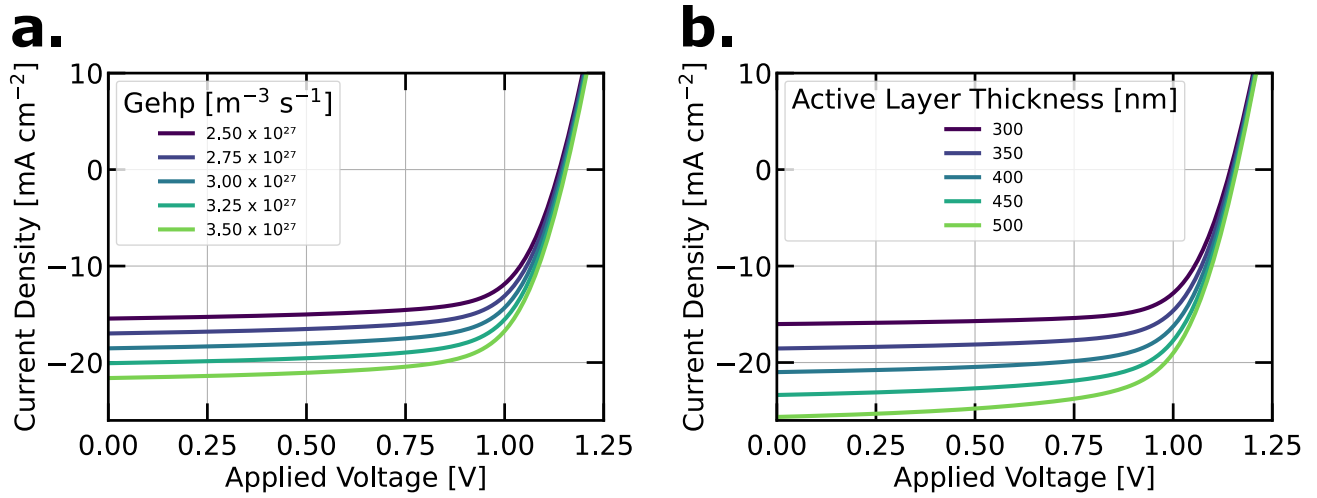


Figure S3: Influence of the (a) electron-hole pair generation rate and (b) active layer thickness on the JVs

OSC:

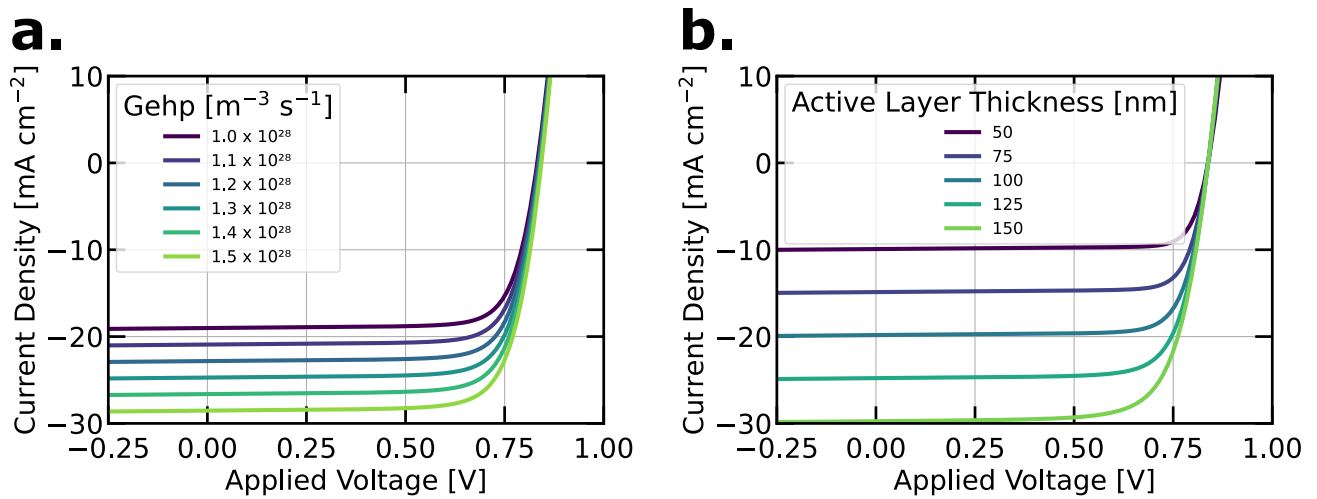


Figure S4: Influence of the (a) electron-hole pair generation rate and (b) active layer thickness on the JVs

II Shunt resistance losses:

PSC:

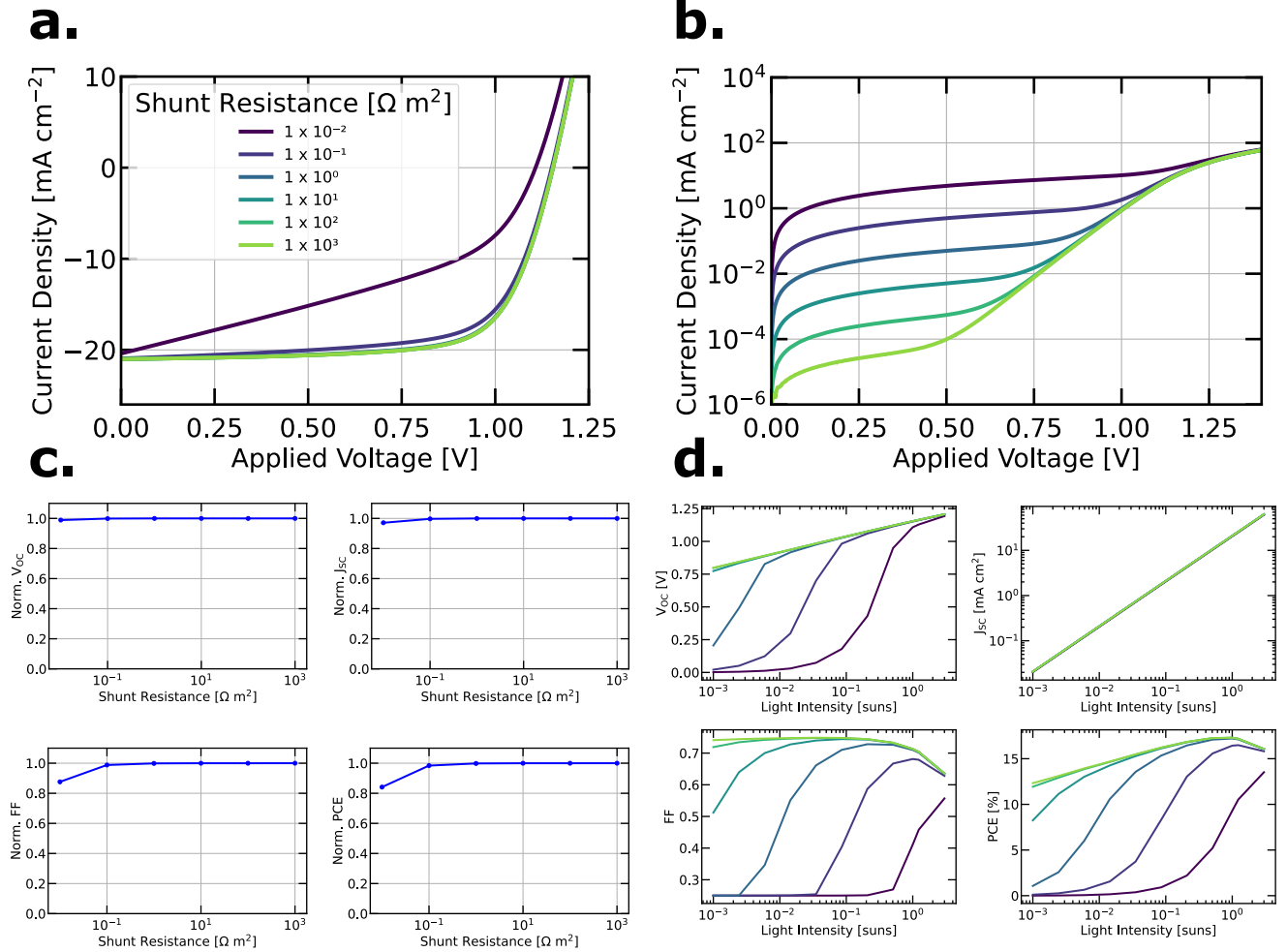


Figure S5: Influence of shunt resistance on the (a) light and (b) dark JVs, (c) 1 sun and (d) light-intensity dependent performances.

OSC:

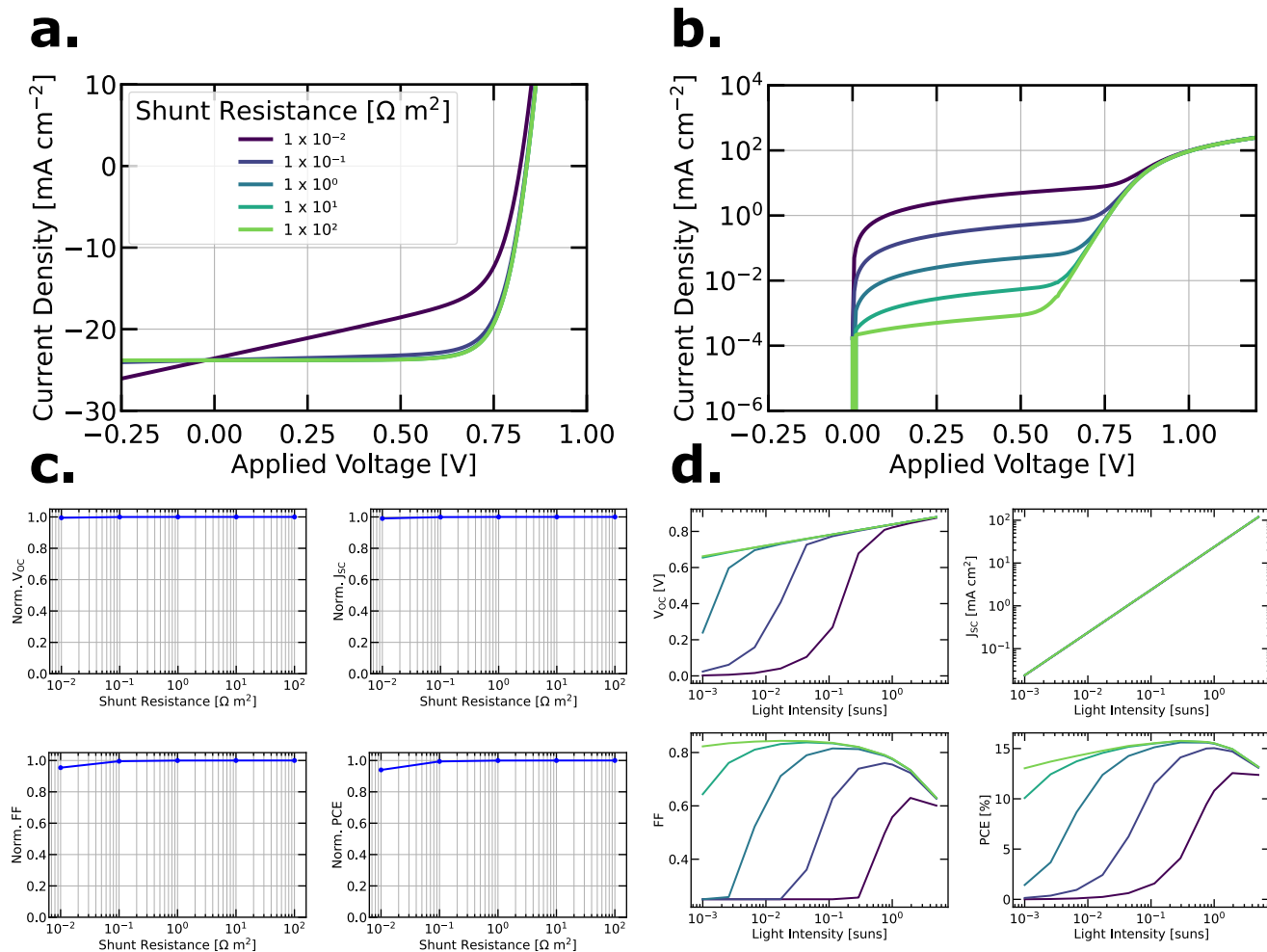


Figure S6: Influence of shunt resistance on the (a) light and (b) dark JVs, (c) 1 sun and (d) light-intensity dependent performances.

III Recombination losses:

PSC:

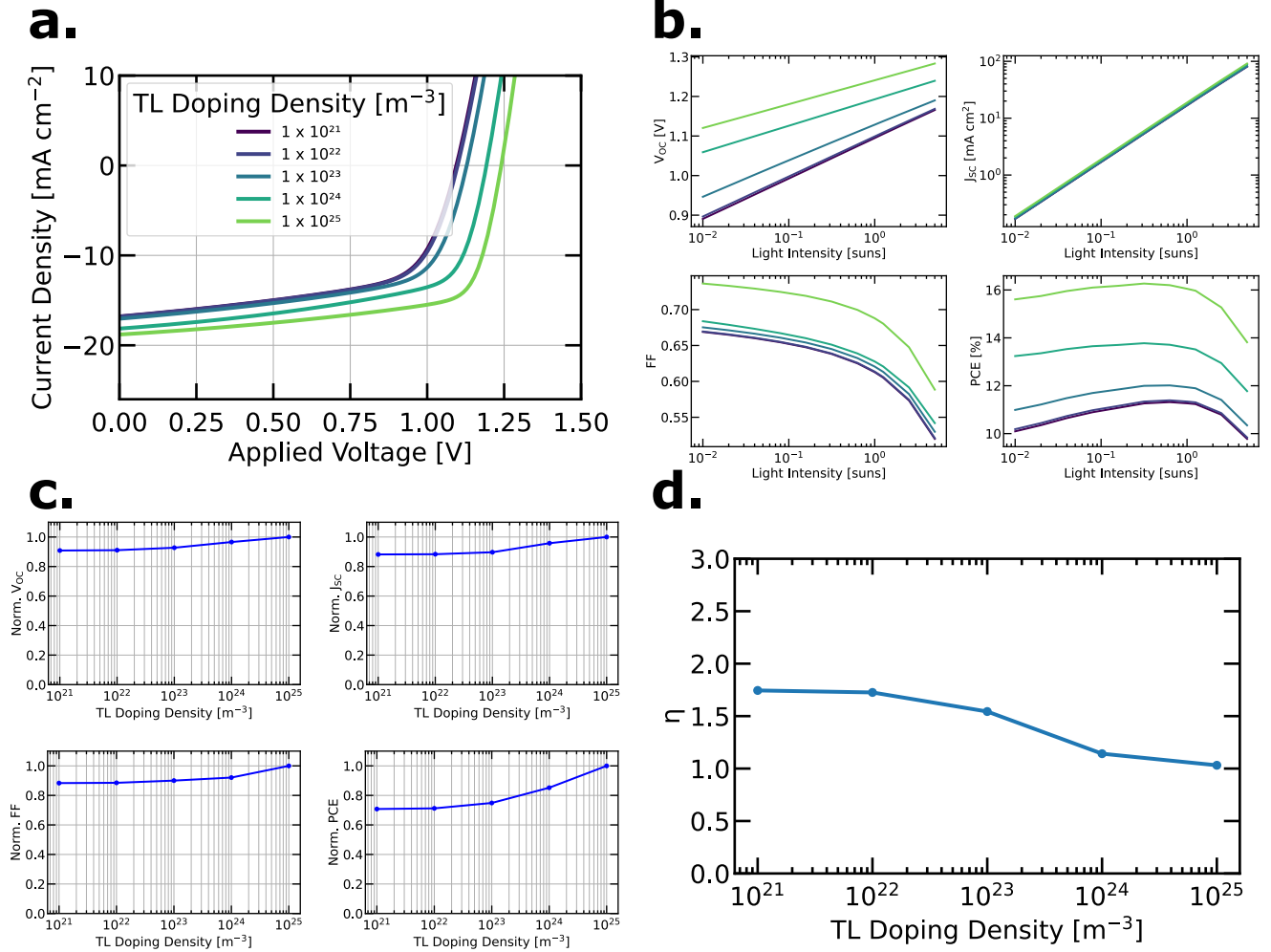


Figure S7: Influence of Fermi level pinning due to doping in the TL on the (a) light JVs, (b) light-intensity dependent and (c) 1 sun performances, (d) ideality factor.

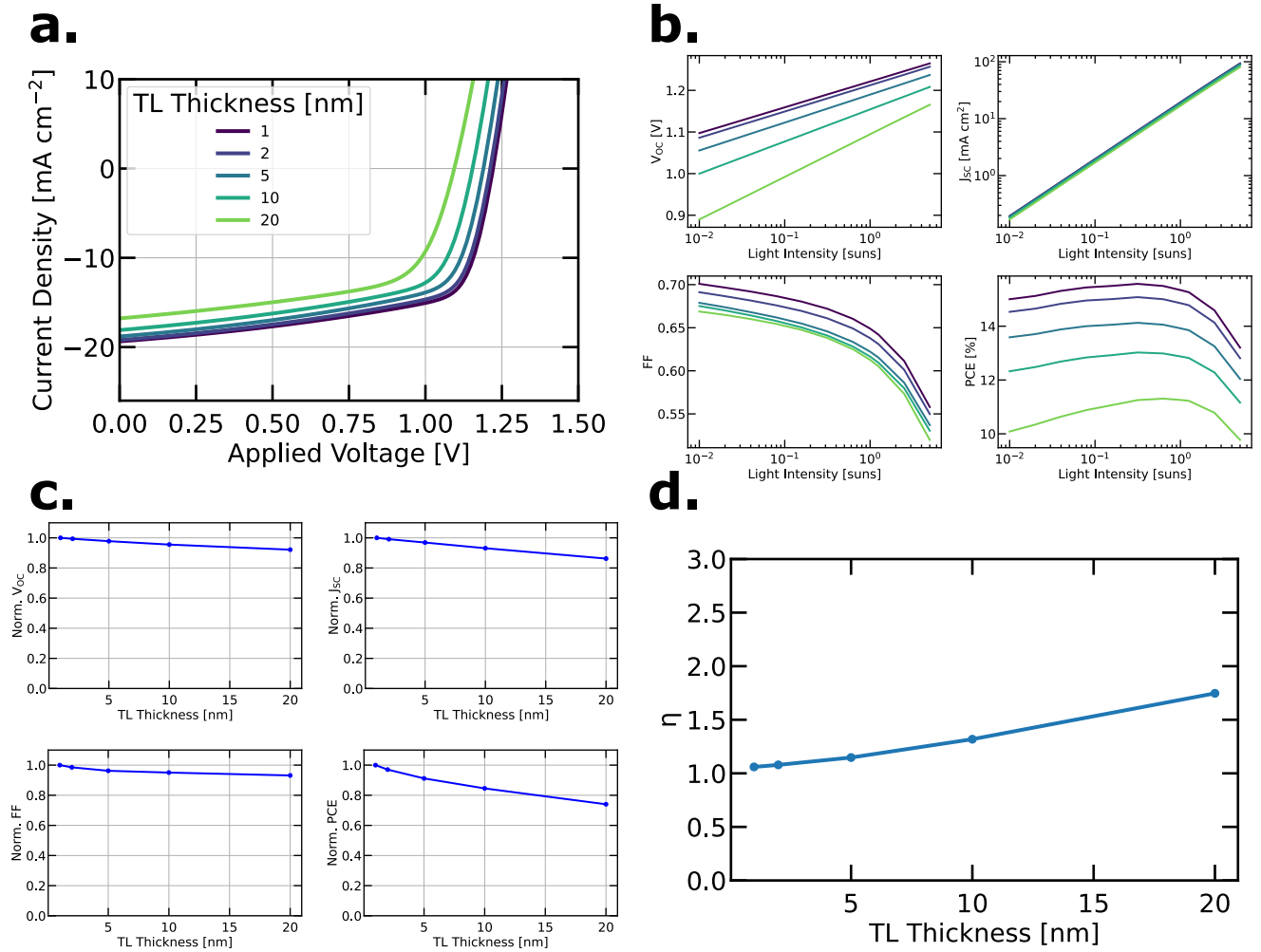


Figure S8: Influence of Fermi level pinning due to TL thickness on the (a) light JVs, (b) light-intensity dependent and (c) 1 sun performances, (d) ideality factor.

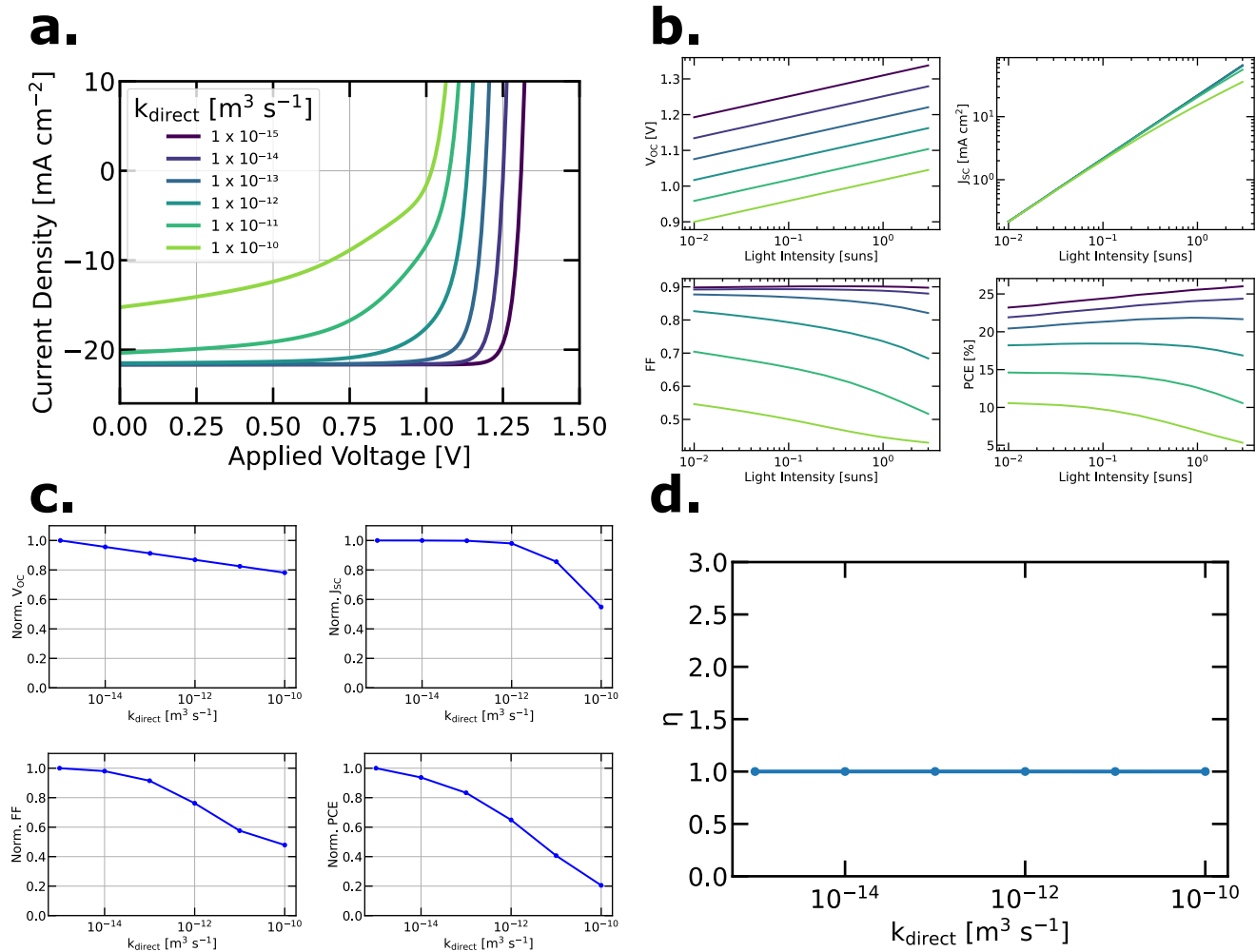


Figure S9: Influence of the band-to-band/bimolecular recombination rate (k_2) on the (a) light JVs, (b) light-intensity dependent and (c) 1 sun performances, (d) ideality factor.

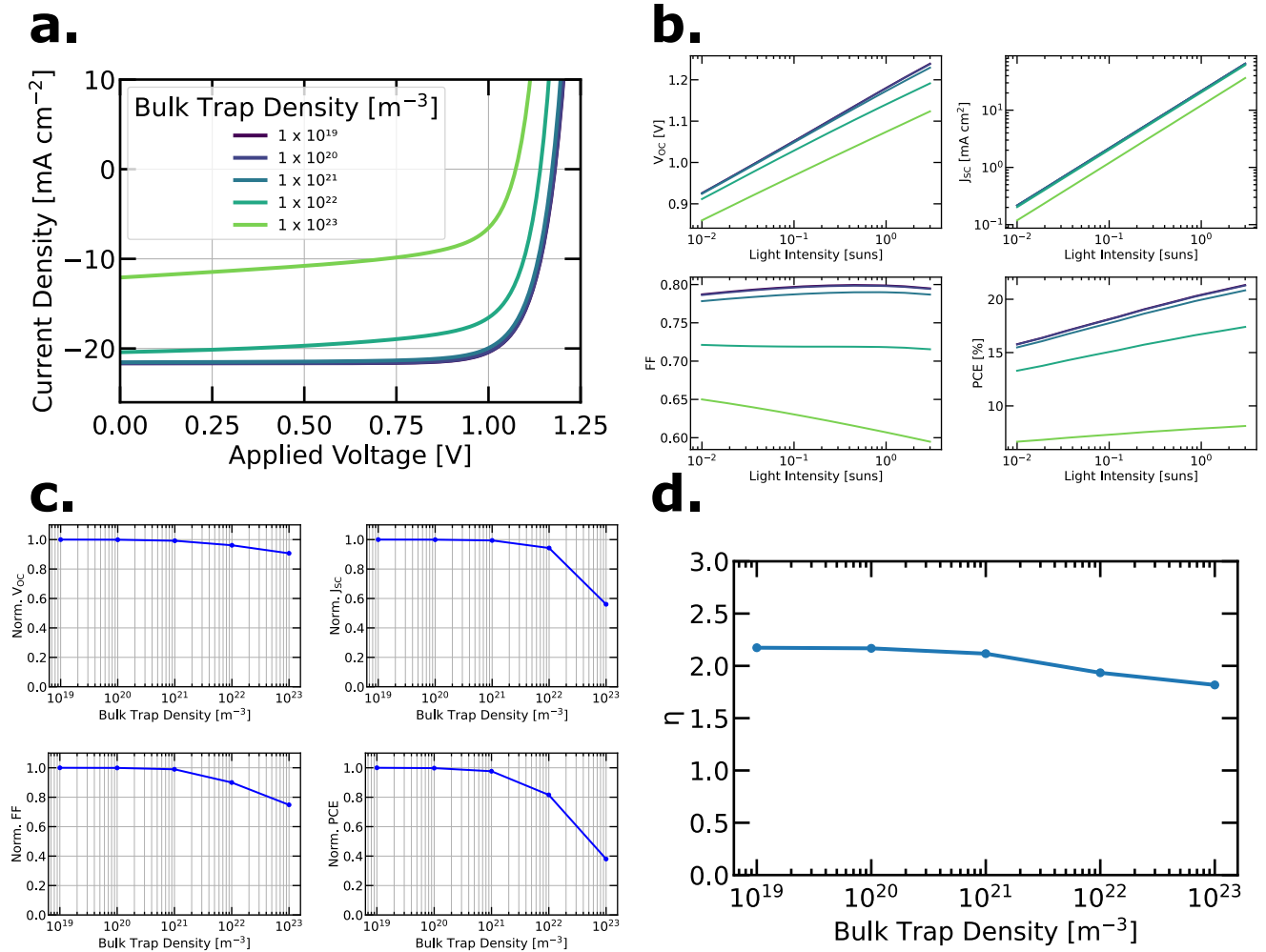


Figure S10: Influence of the bulk trap density on the (a) light JVs, (b) light-intensity dependent and (c) 1 sun performances, (d) ideality factor.

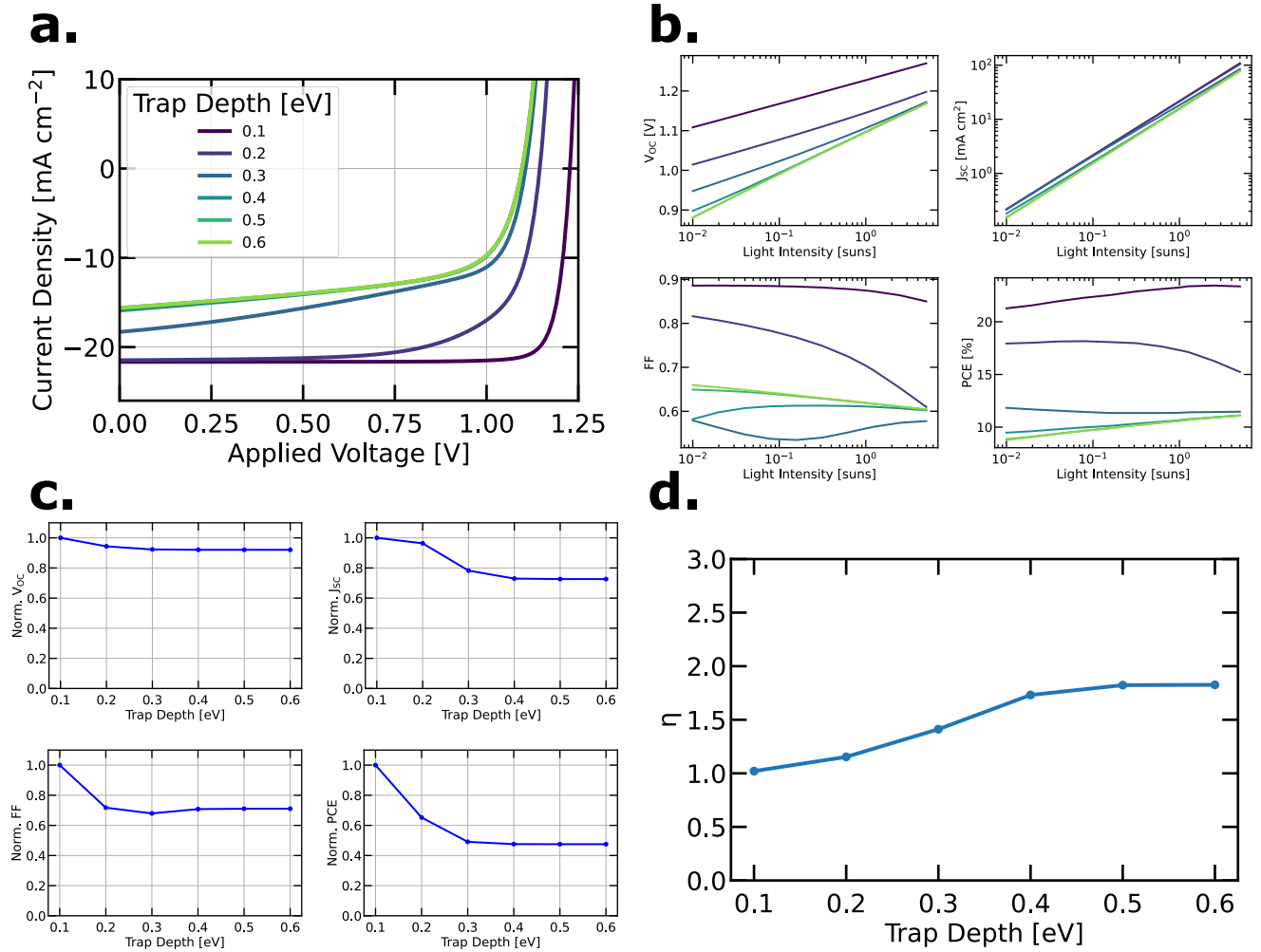


Figure S11: Influence of the trap level depth on the (a) light JVs, (b) light-intensity dependent and (c) 1 sun performances, (d) ideality factor.

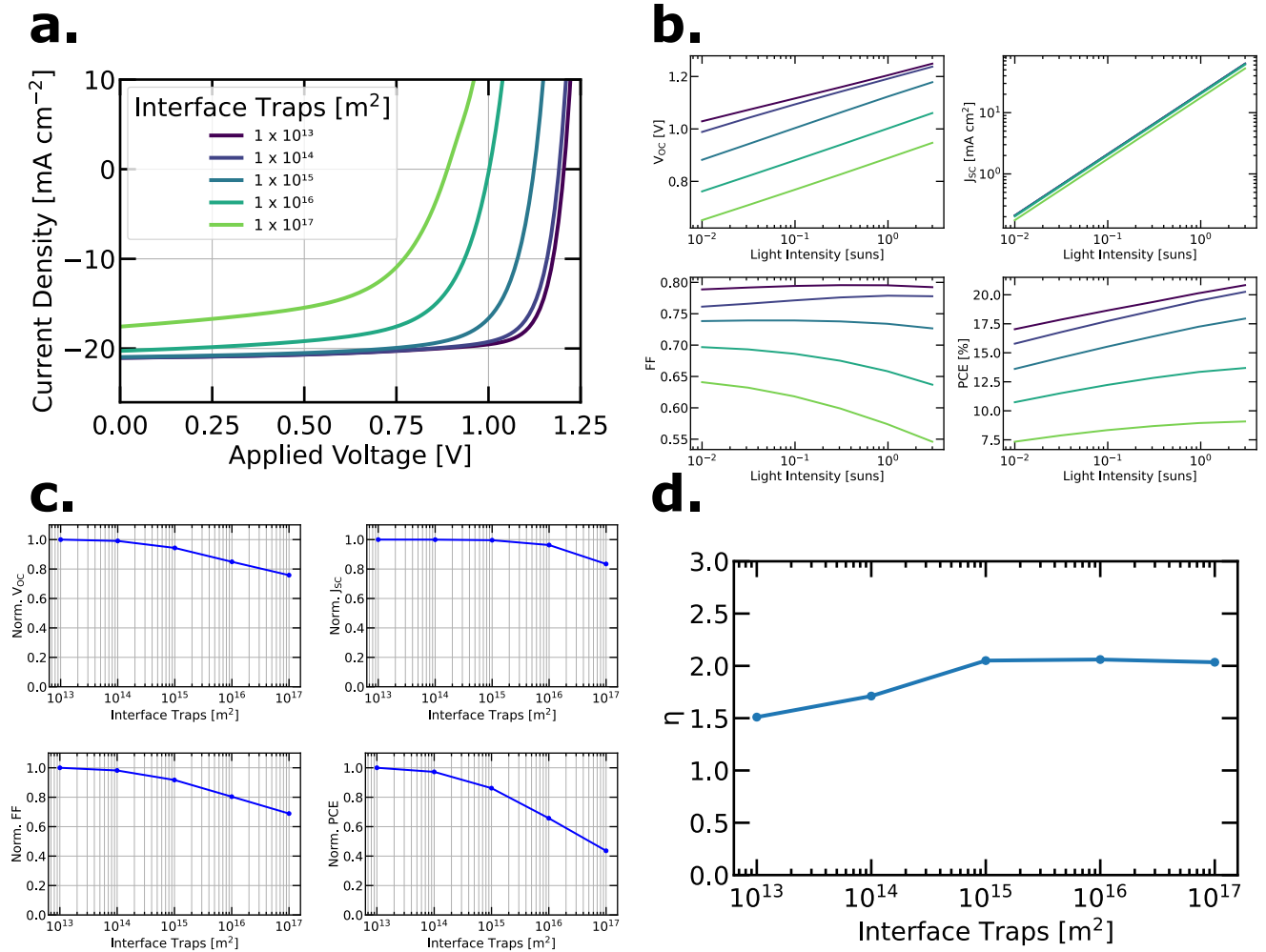


Figure S12: Influence of the interface trap density on the (a) light JVs, (b) light-intensity dependent and (c) 1 sun performances, (d) ideality factor.

OSC:

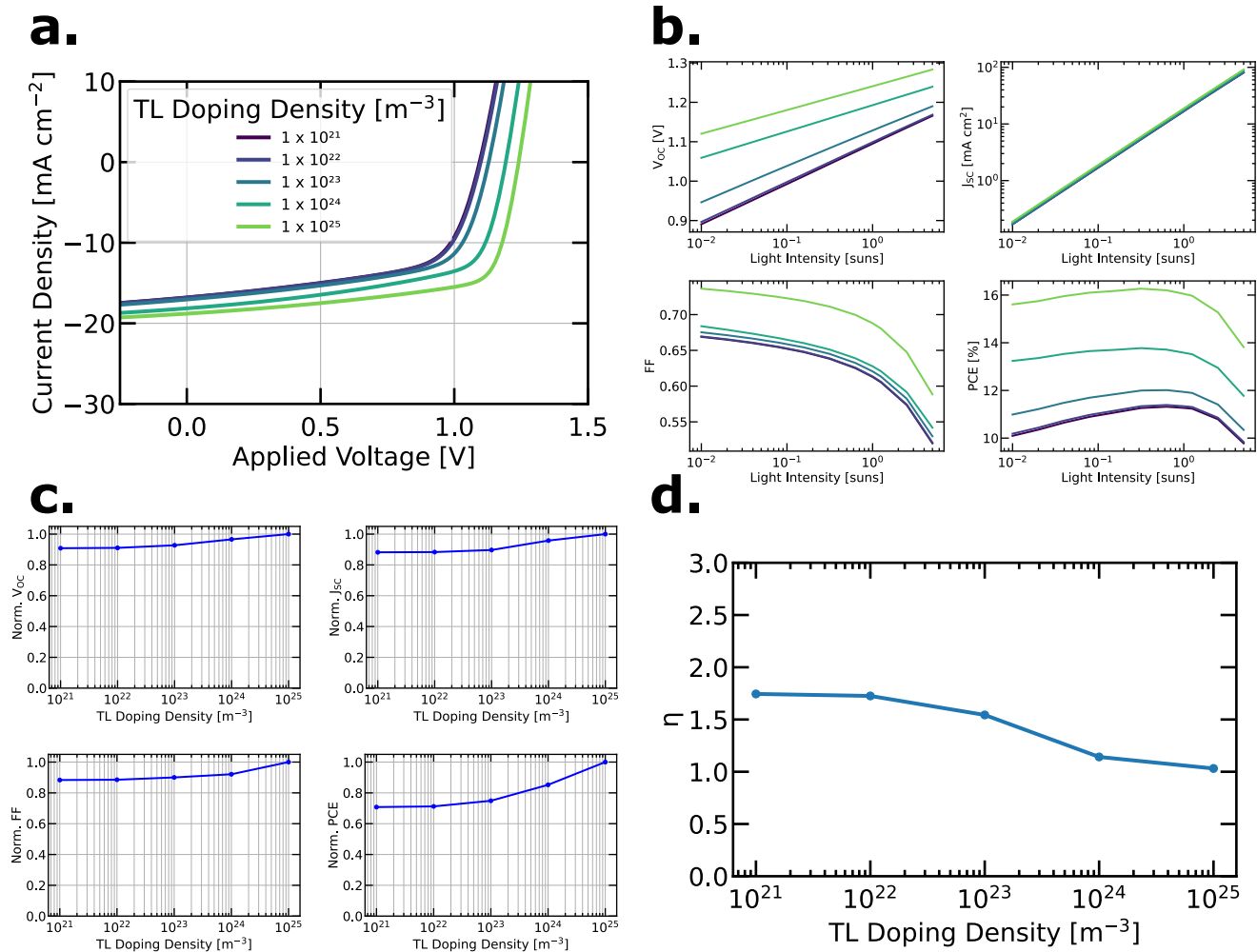


Figure S13: Influence of Fermi level pinning due to doping in the TL on the (a) light JVs, (b) light-intensity dependent and (c) 1 sun performances, (d) ideality factor.

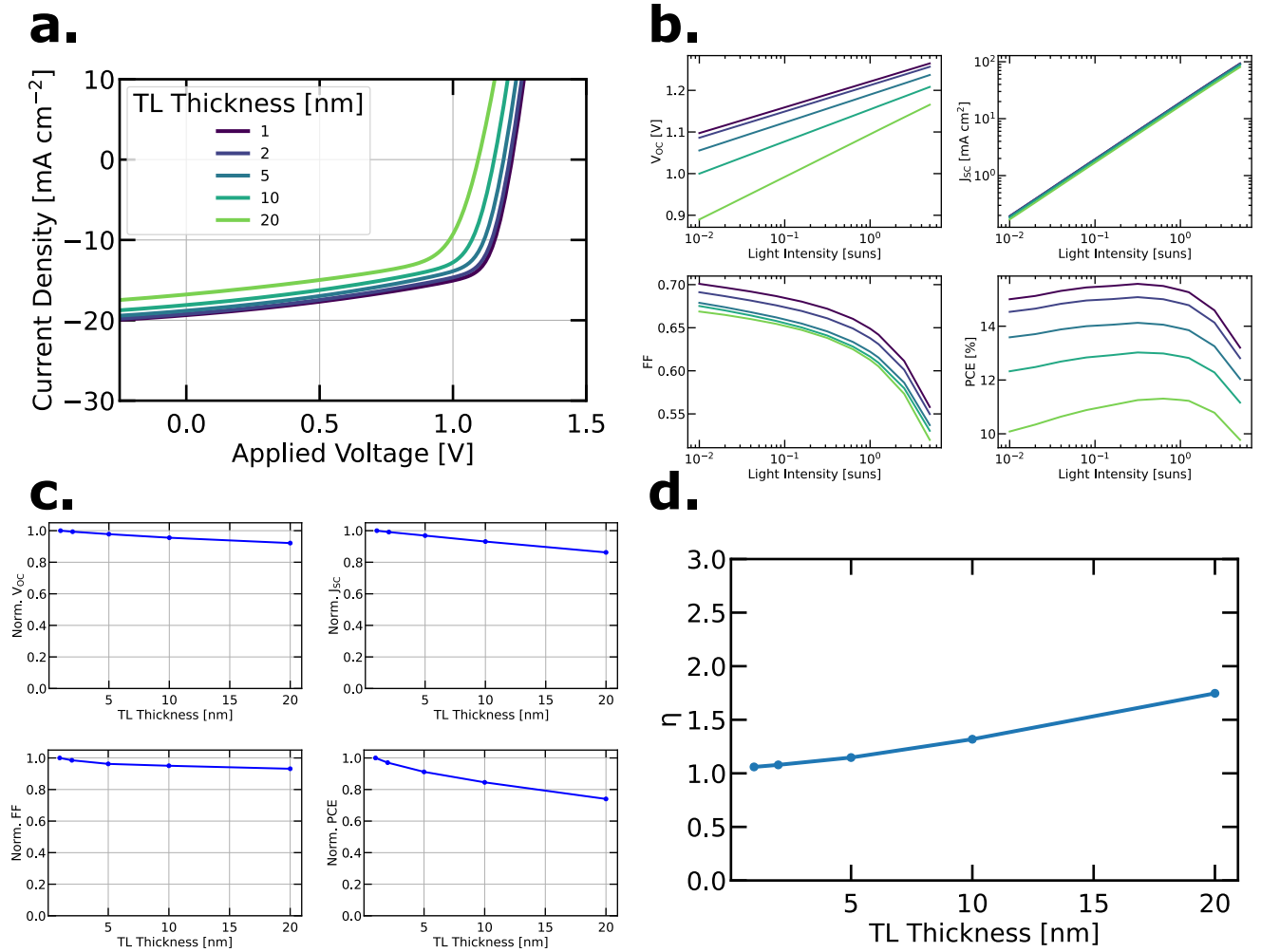


Figure S14: Influence of Fermi level pinning due to TL thickness on the (a) light JVs, (b) light-intensity dependent and (c) 1 sun performances, (d) ideality factor.

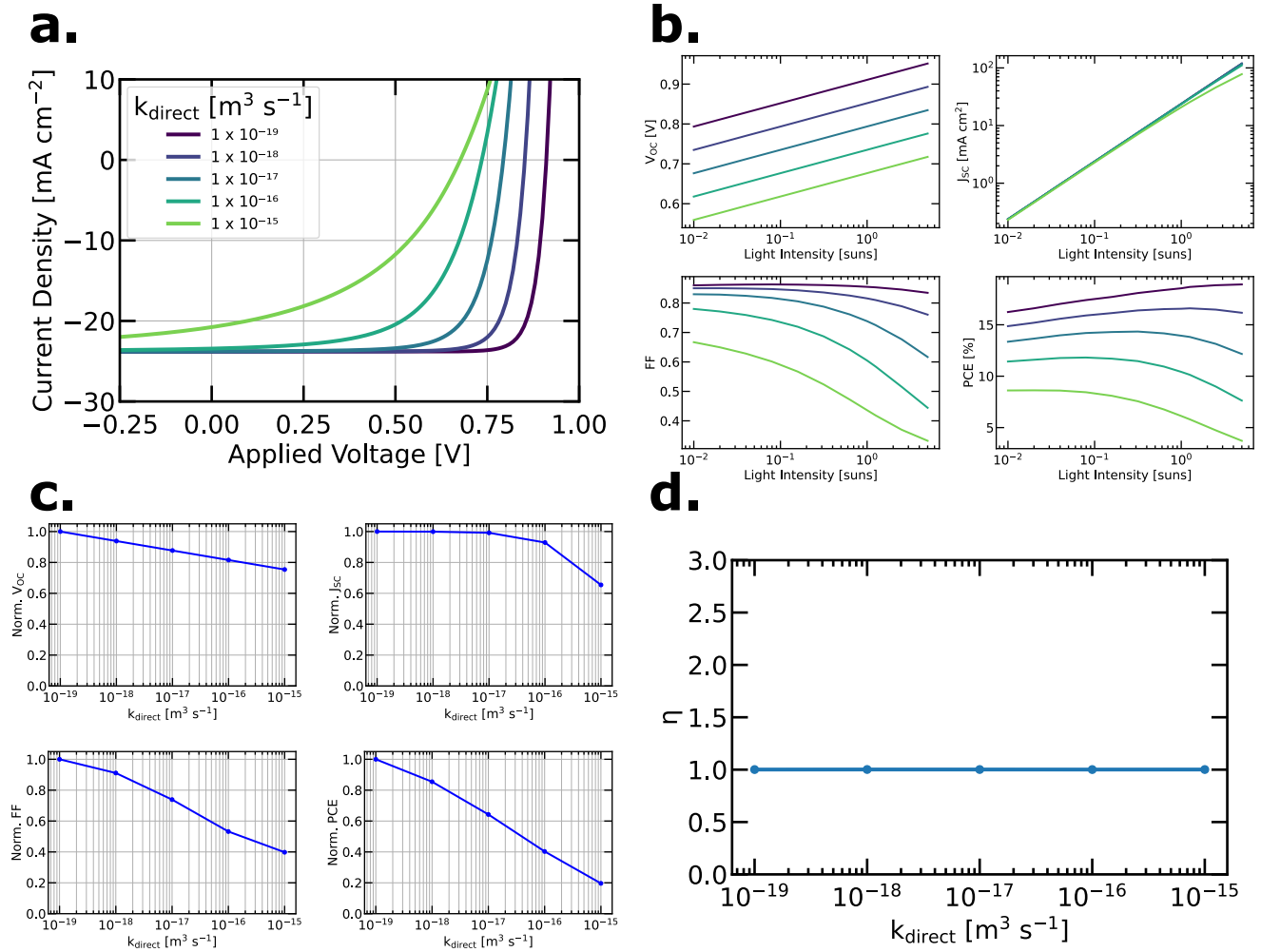


Figure S15: Influence of the band-to-band/bimolecular recombination rate (k_2) on the (a) light JVs, (b) light-intensity dependent and (c) 1 sun performances, (d) ideality factor.

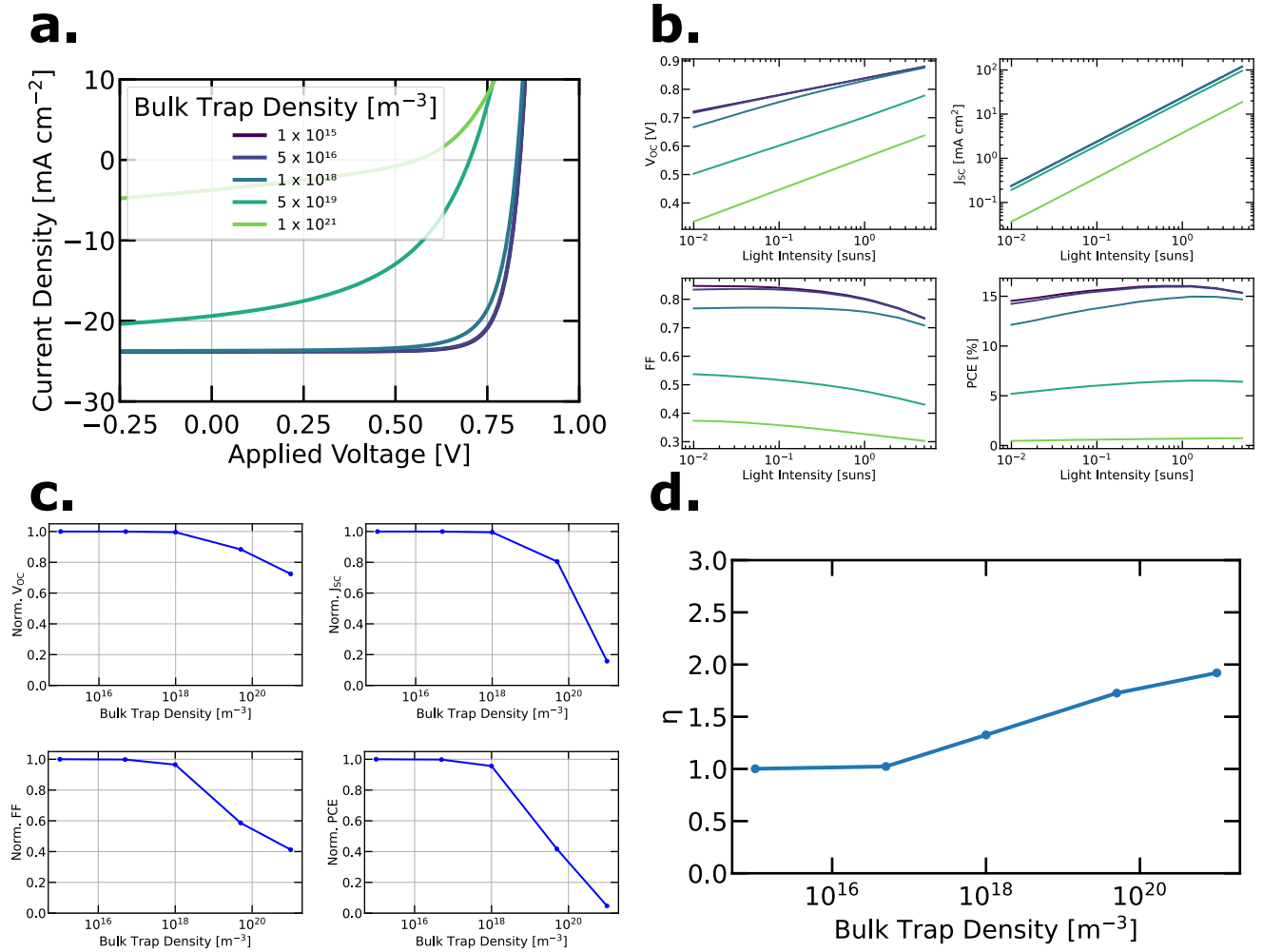


Figure S16: Influence of the bulk trap density on the (a) light JVs, (b) light-intensity dependent and (c) 1 sun performances, (d) ideality factor.

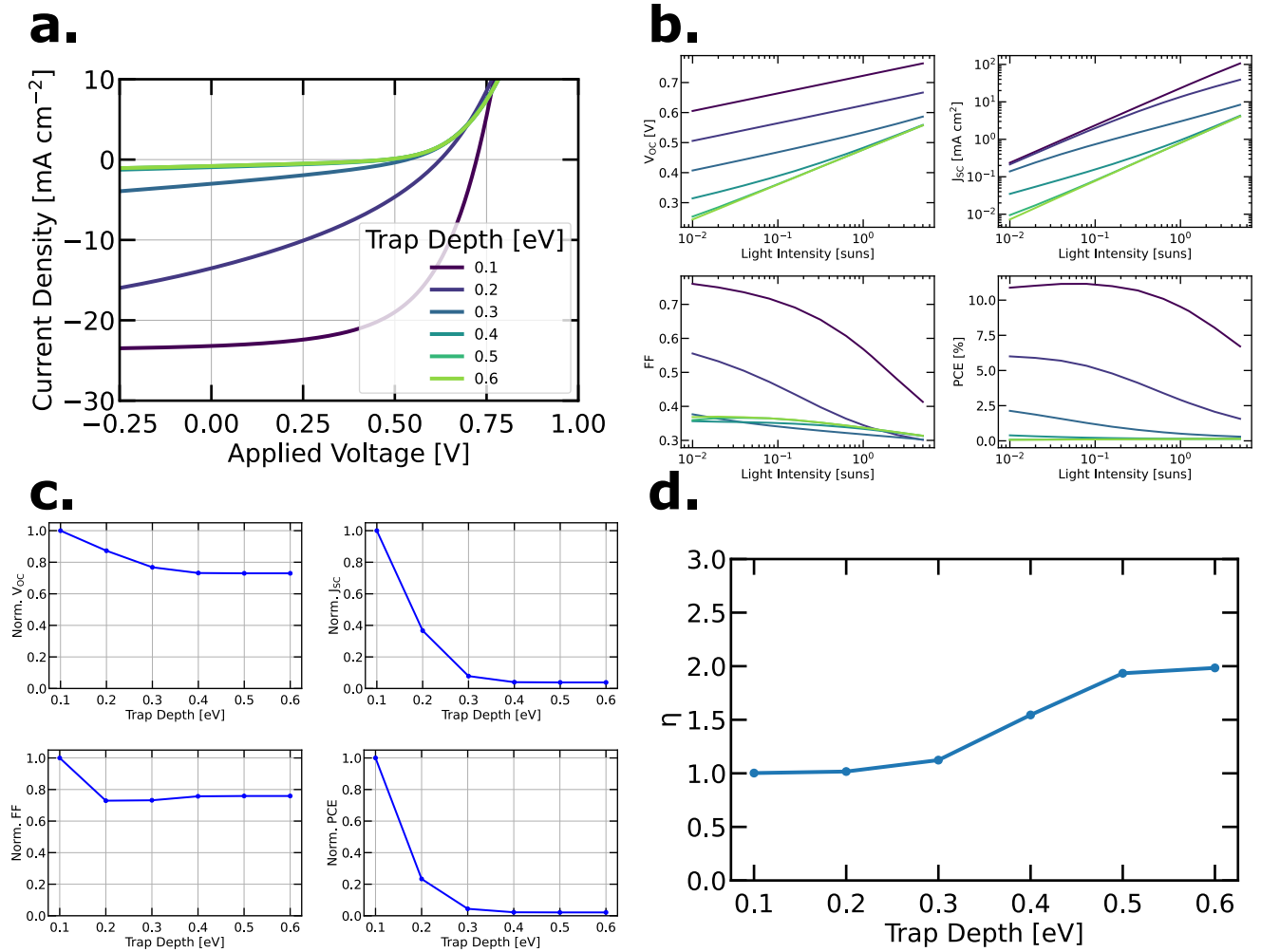


Figure S17: Influence of the trap level depth on the (a) light JVs, (b) light-intensity dependent and (c) 1 sun performances, (d) ideality factor.

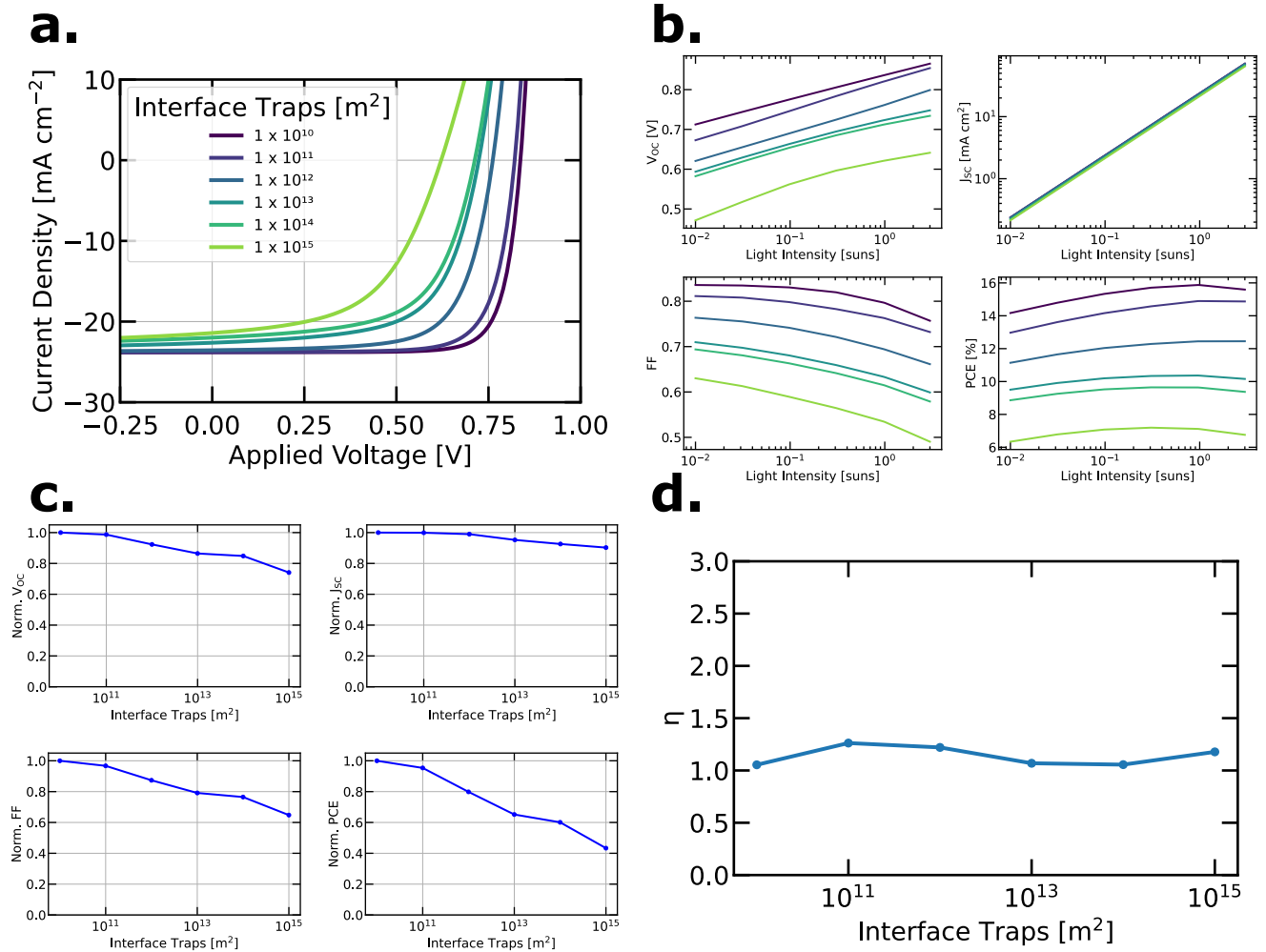


Figure S18: Influence of the interface trap density on the (a) light JVs, (b) light-intensity dependent and (c) 1 sun performances, (d) ideality factor.

IV Injection barrier and trapping at the transport layer to active layer interface losses:

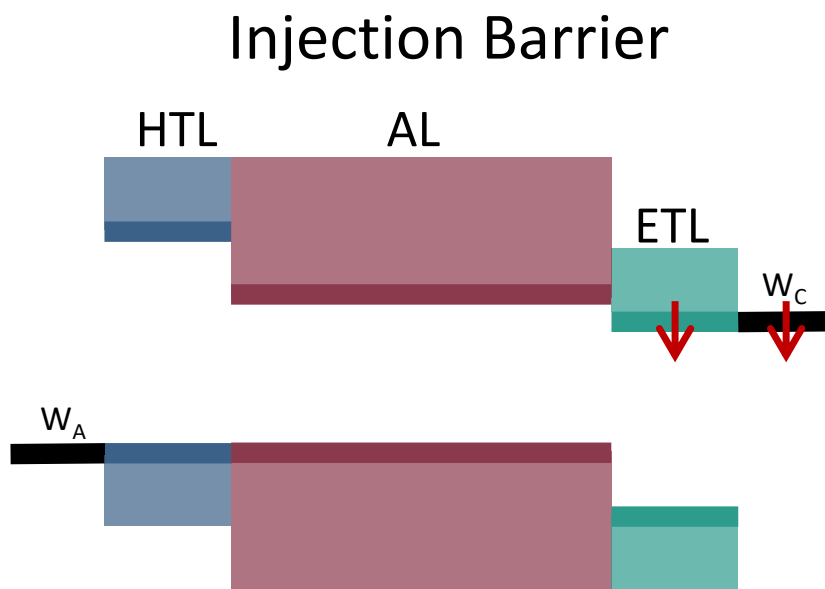


Figure S19: Sketch showing the energy band diagrams for the injection barrier

PSC:

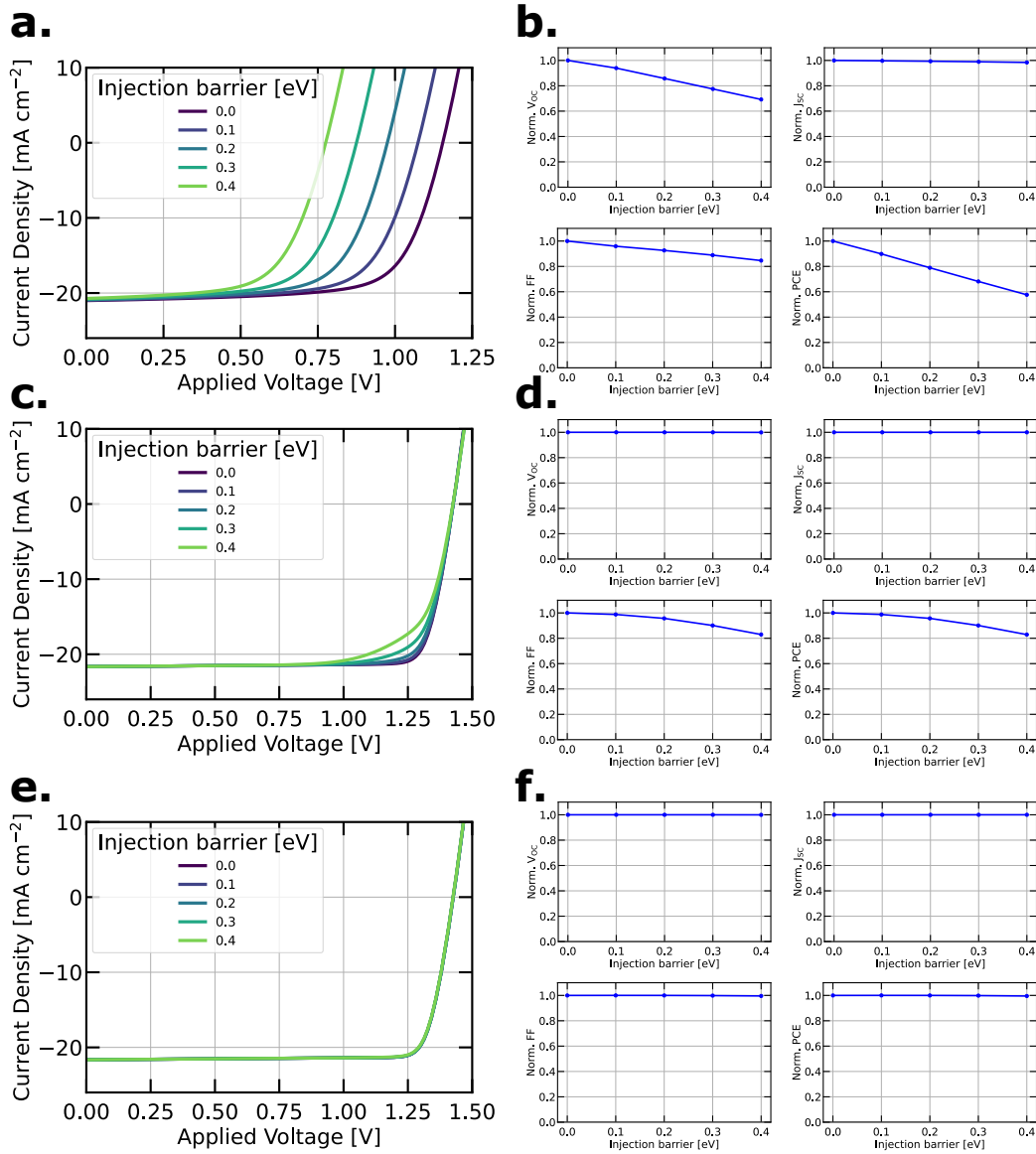


Figure S20: Influence of the injection barrier from the transport layer to the active layer with (a-b) and without (c-f) interfacial trapping on JVS and 1 sun performances. The injection barrier in the absence of trapping only reduced the FF , if the AL electron mobility is low (c-d), otherwise the performance is not affected (e-f)

OSC:

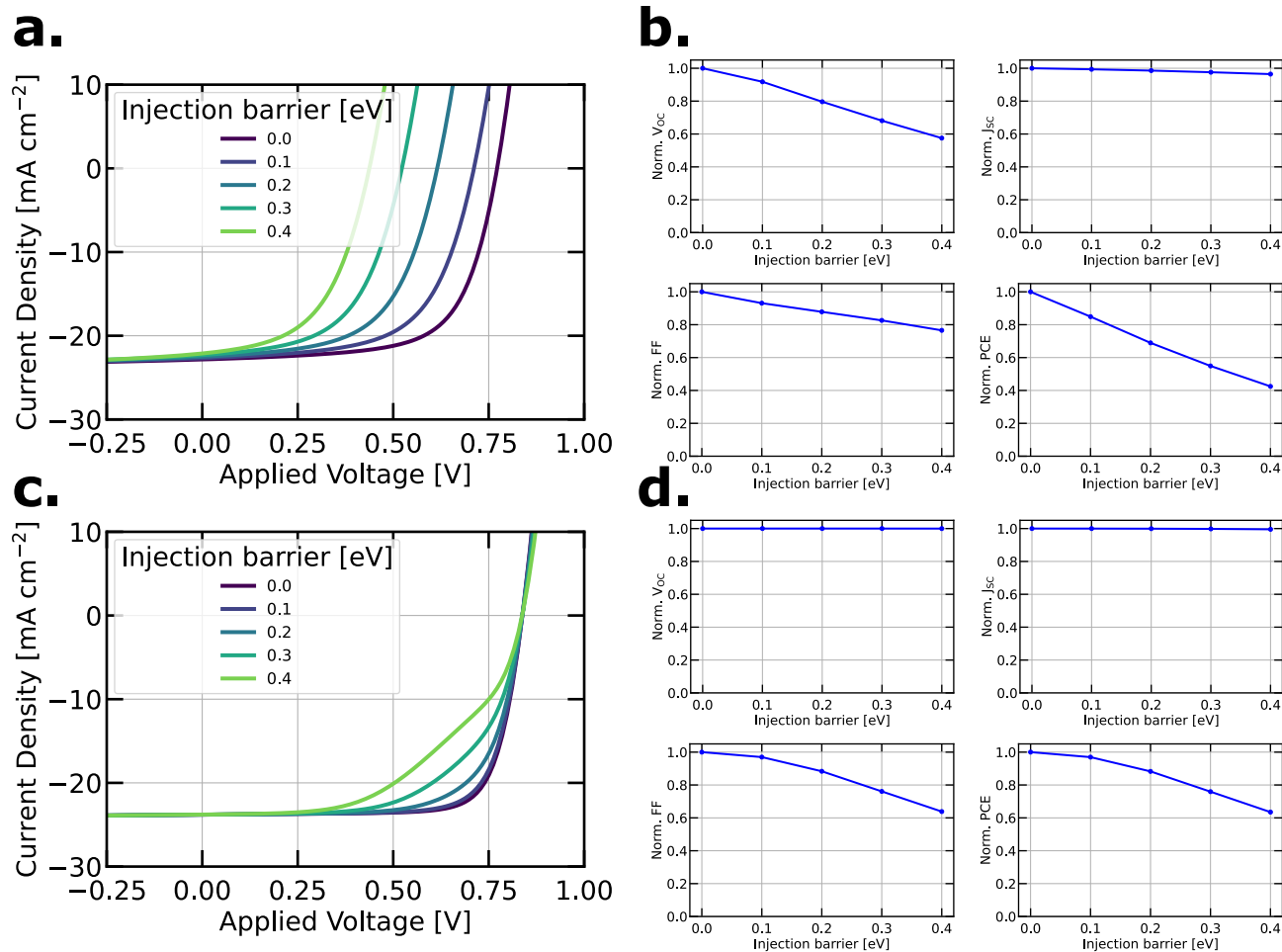


Figure S21: Influence of the injection barrier from the transport layer to the active layer with (a-b) and without (c-d) interfacial trapping on JVs and 1 sun performances. The injection barrier in the absence of trapping does reduce the FF of.

V Ionic losses:

PSC:

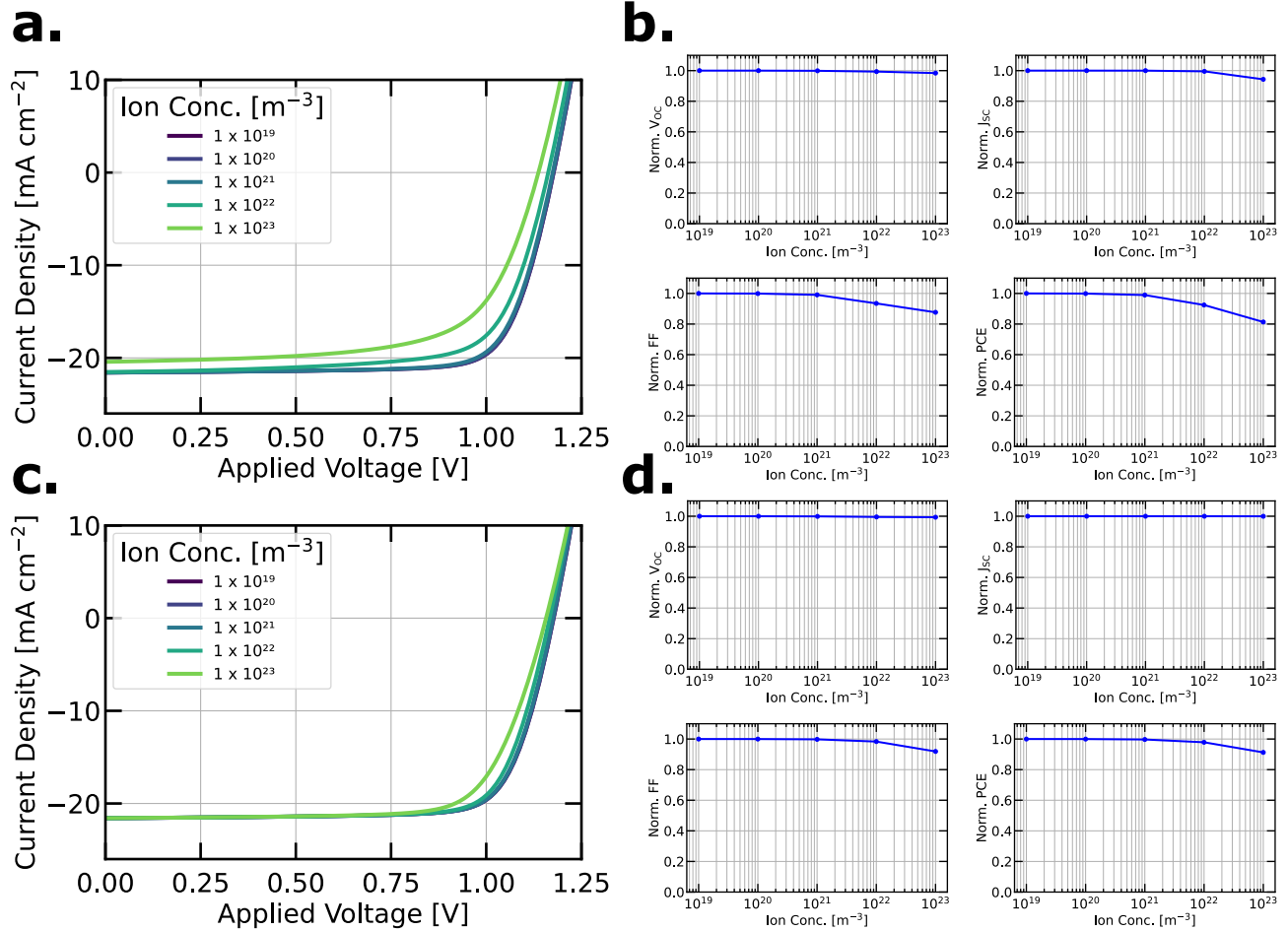


Figure S22: Influence of the concentration of positively and negatively charged ions ($I_n = I_p$) on JVs (a,c) and performance parameters (b,d). (a-b) Ions cannot move into the transport layer, (c-d) ions can move into the transport layer.

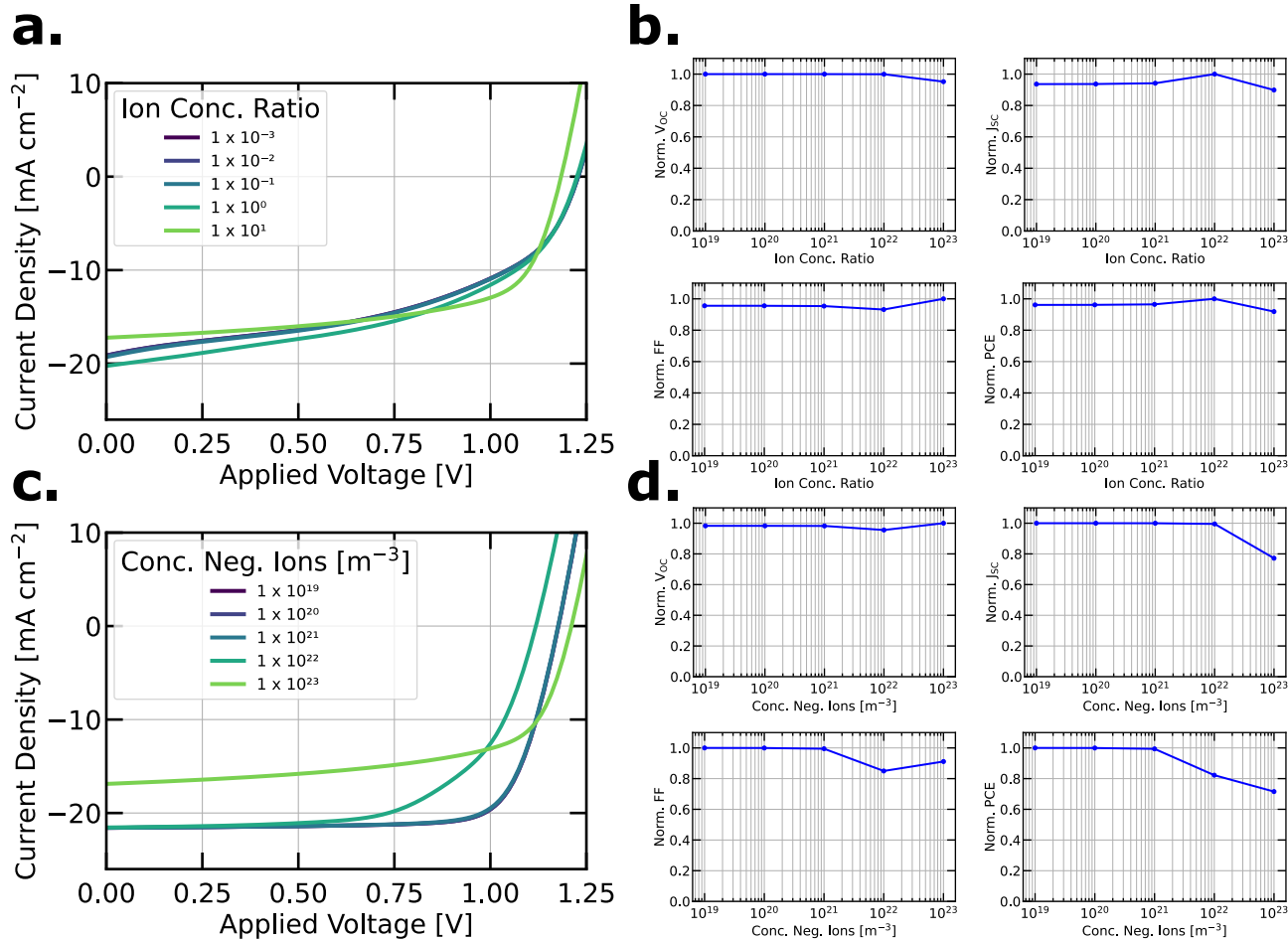


Figure S23: Influence of concentration of positively and negatively charged ions (a-b) ion ratio $\frac{I_n}{I_p}$, with $I_p = 1 \times 10^{22} \text{ m}^{-3}$ and (c-d) I_n with $I_p = 0 \text{ m}^{-3}$ on the JVs. Ions cannot move into the transport layers.

VI Field-dependant generation losses:

OSC:

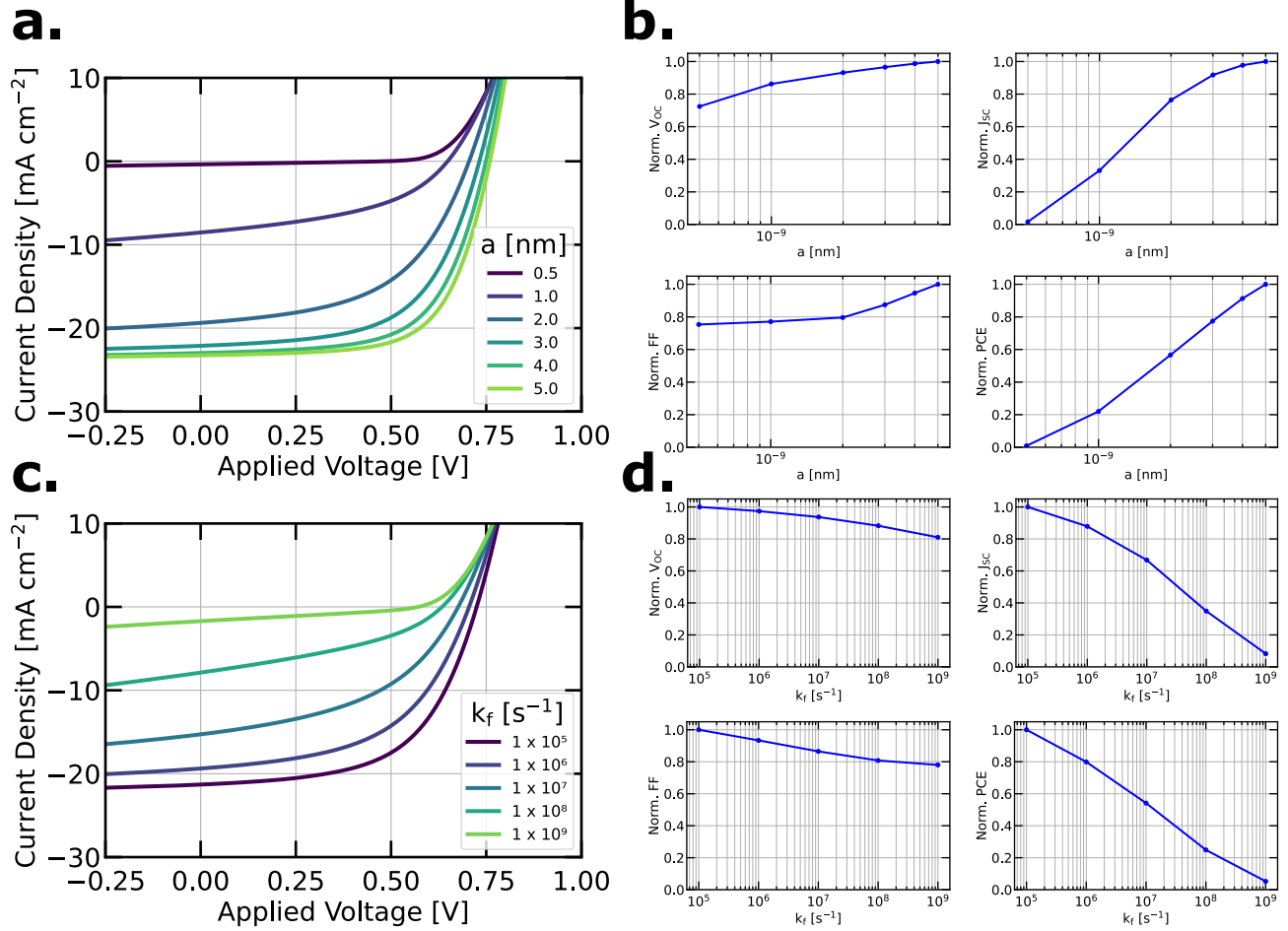


Figure S24: Influence of field-dependent charge generation losses on the JVs and 1 sun performances. (a-b) shows the impact of the initial separation of bound charge carriers at the donor-acceptor interface a and (c-d) the geminate recombination rate k_f .

VII Series resistance losses:

PSC:

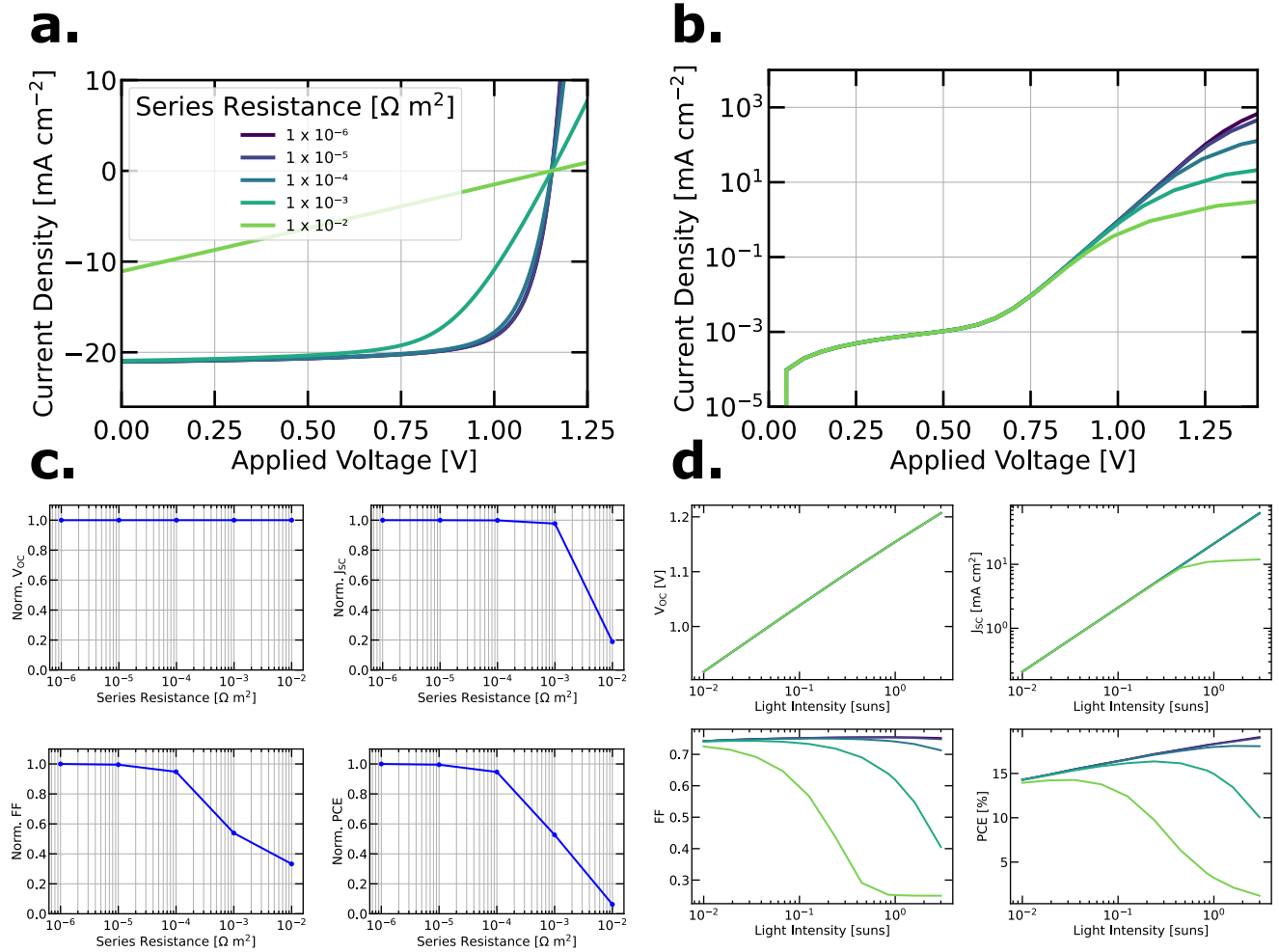


Figure S25: Influence of series resistance on the (a) light and (b) dark JVs, (c) 1 sun and (d) light-intensity dependent performances.

OSC:

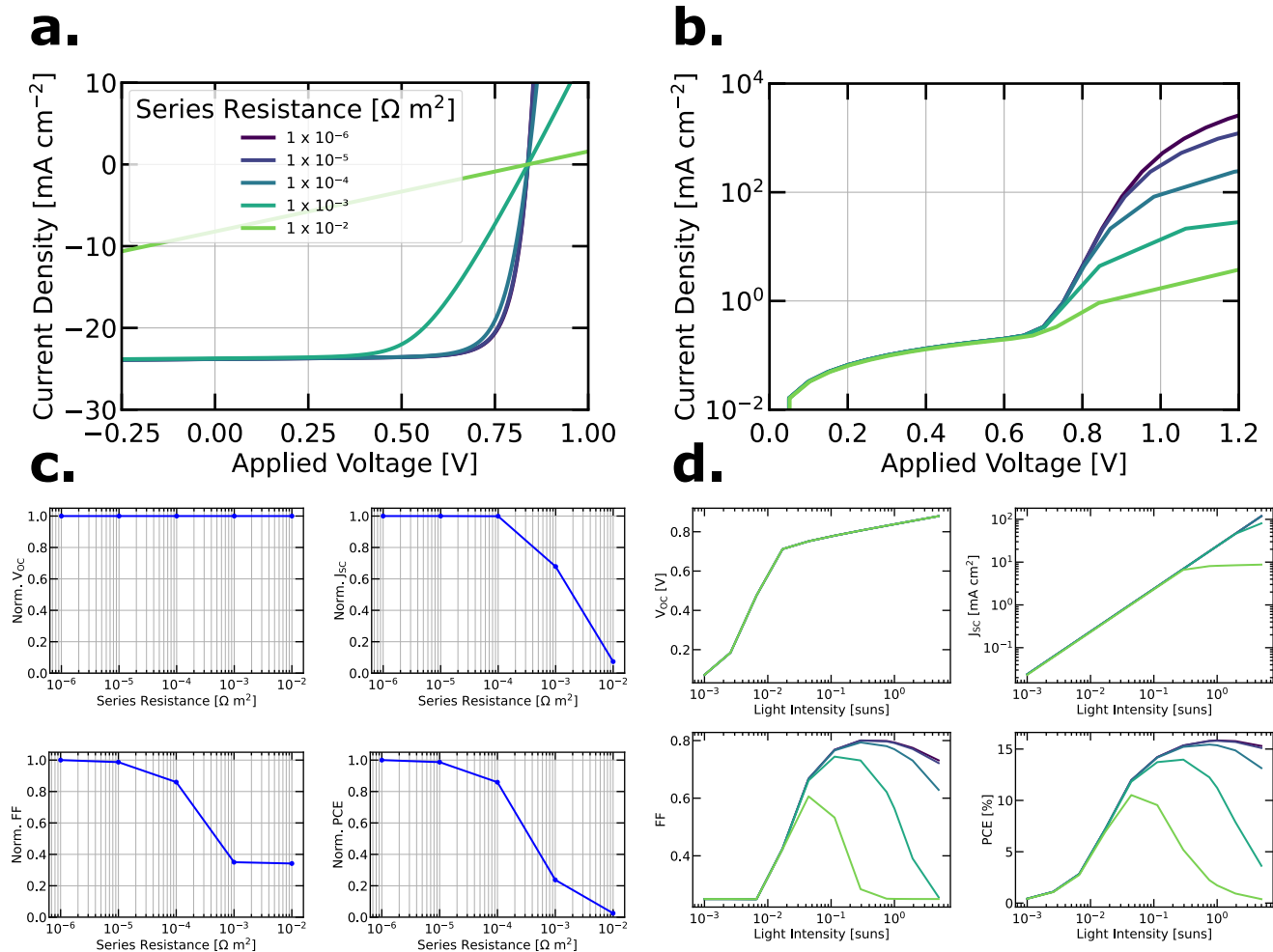


Figure S26: Influence of series resistance on the (a) light and (b) dark JVs, (c) 1 sun and (d) light-intensity dependent performances.

VIII Extraction and transport losses:

PSC:

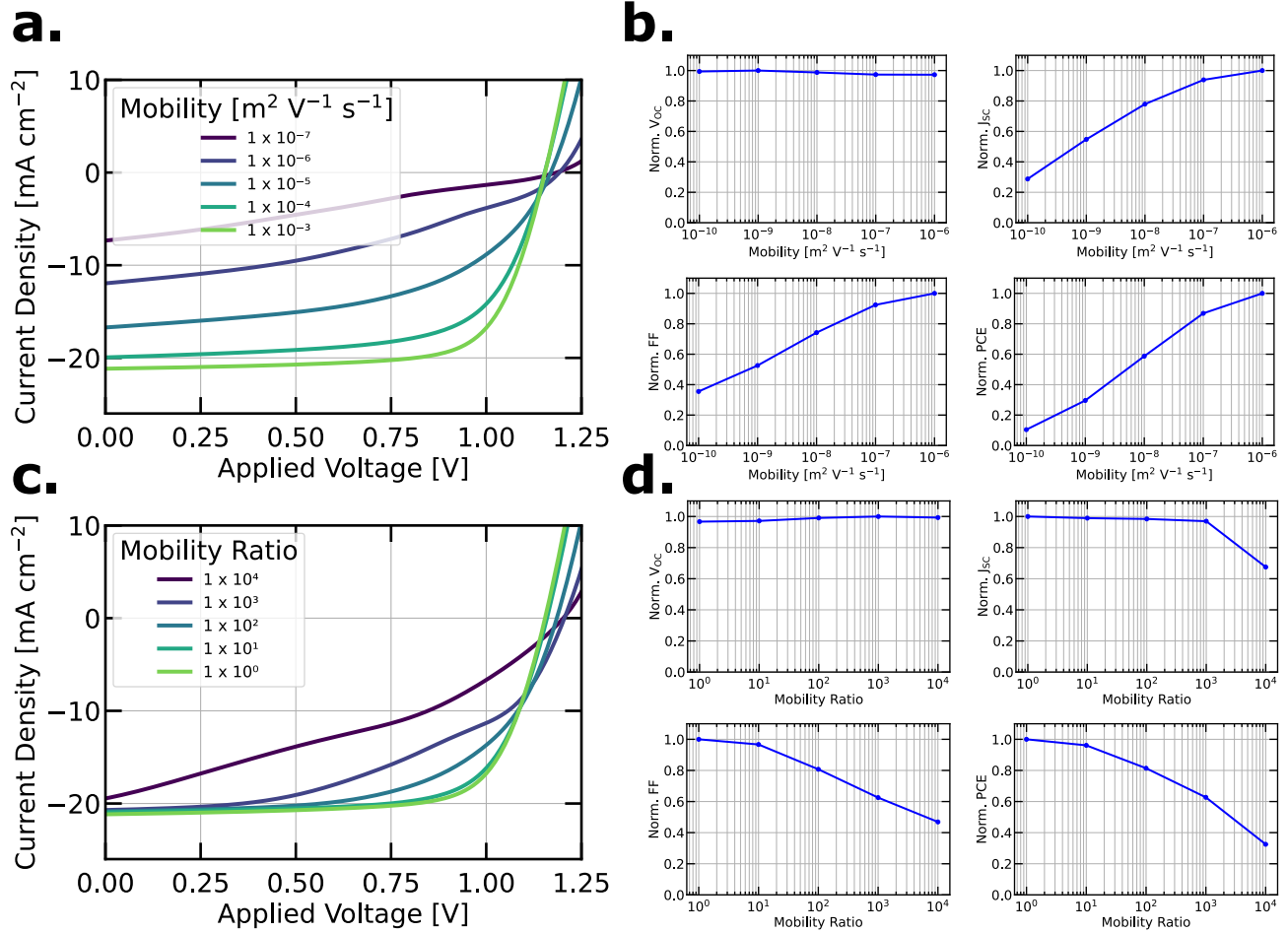


Figure S27: Influence of (a-b) active layer mobility ($\mu_n = \mu_p$) and (c-d) mobility ratio ($ratio = \frac{\mu_n}{\mu_p}$) on JVs and 1 sun performances.

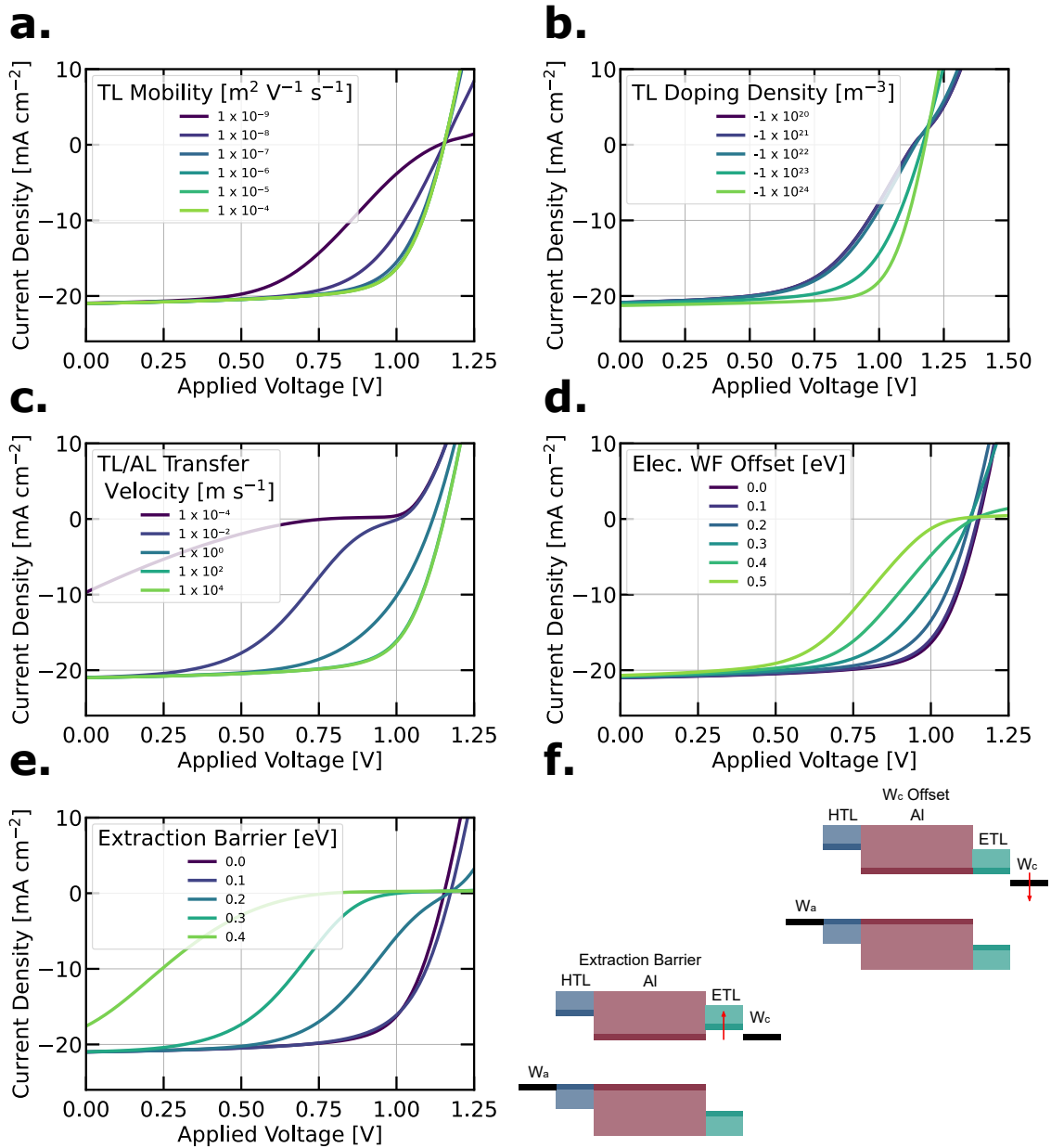


Figure S28: Influence of transport layer (a) mobility and (b) doping, (c) transfer velocity at the transport layer/active layer interface, (d) electrode work function offset (i.e. injection barrier), (e) extraction barrier from the active layer to the transport layer on the current-voltage characteristics. (f) Sketch showing the energy band diagrams showing for (d) and (e) respectively

OSC:

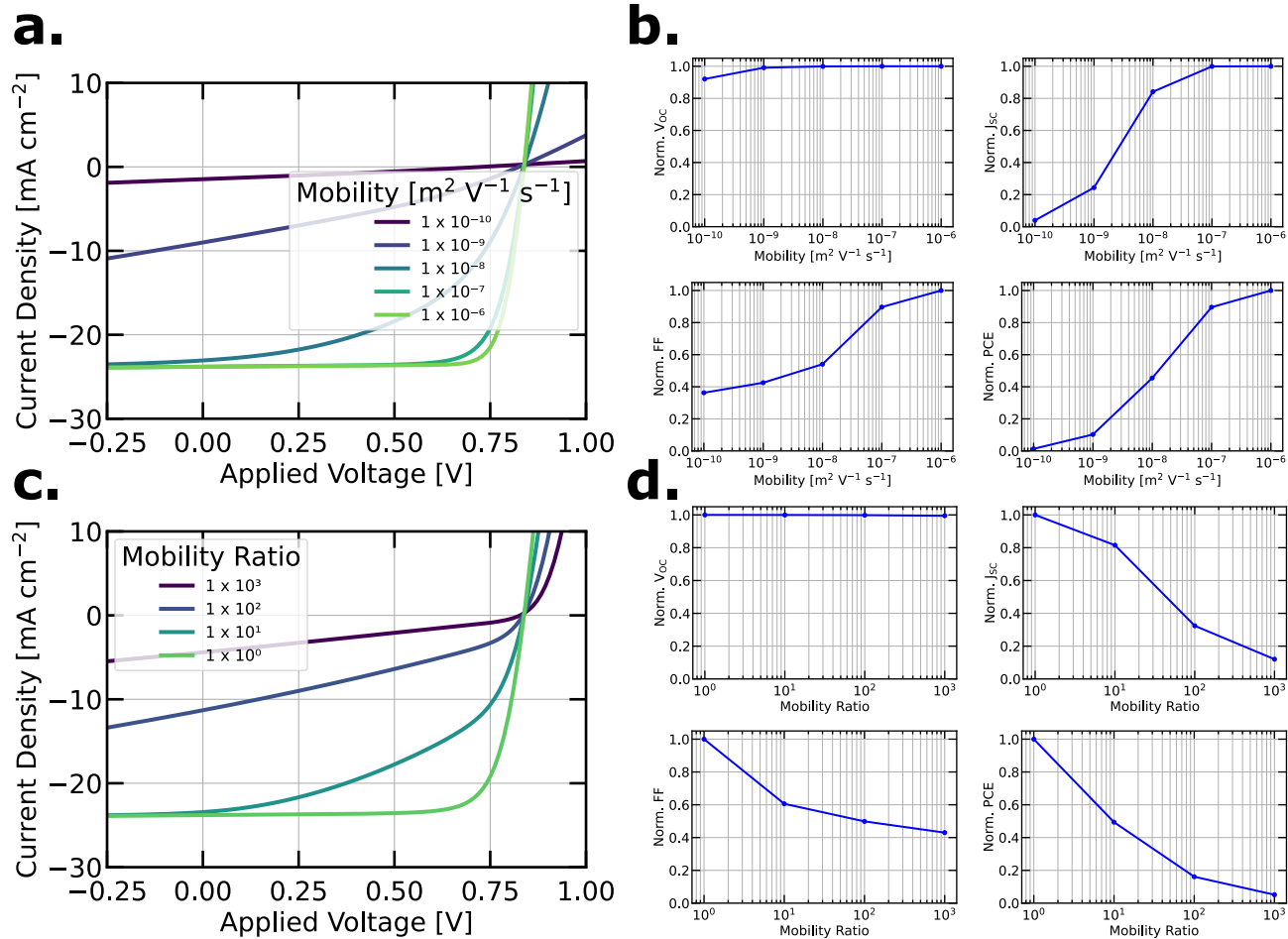


Figure S29: Influence of (a-b) active layer mobility ($\mu_n = \mu_p$) and (c-d) mobility ratio ($ratio = \frac{\mu_n}{\mu_p}$) on JVs and 1 sun performances.

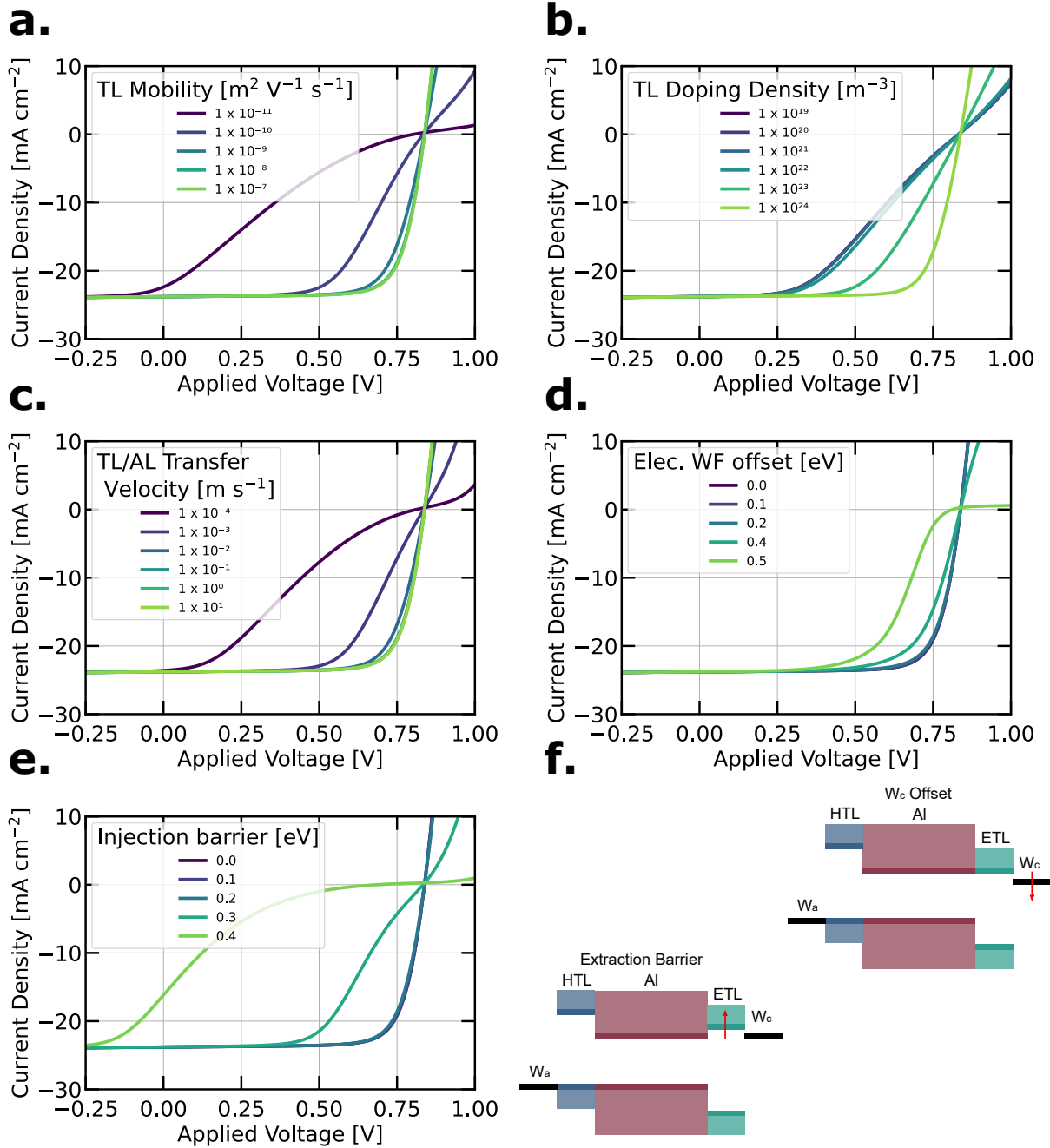


Figure S30: Influence of transport layer (a) mobility and (b) doping, (c) transfer velocity at the transport layer/active layer interface, (d) electrode work function offset (i.e. injection barrier), (e) extraction barrier from the active layer to the transport layer on the current-voltage characteristics. (f) Sketch showing the energy band diagrams showing for (d) and (e) respectively

Simulation Parameters:

Table S1: Parameters used in the base case scenario for the PSC.

Parameter	Symbol	Value
Active Layer		
Conduction band	E_c	3.9 eV
Valence band	E_v	5.53 eV
Band gap	E_{gap}	1.63 eV
Effective density of states	N_{cv}	$1 \times 10^{24} \text{ m}^{-3}$
Thickness	L	400 nm
Electron mobility	μ_n	$7 \times 10^{-4} \text{ m}^2 \text{ V}^{-1} \text{ s}^{-1}$
Hole mobility	μ_p	$7 \times 10^{-4} \text{ m}^2 \text{ V}^{-1} \text{ s}^{-1}$
Relative dielectric constant	ϵ_r	22
Concentration of negative (positive) ions	$I_{n(p)}$	$6 \times 10^{22} \text{ m}^{-3}$
Initial charge separation distance	a	$1 \times 10^{-9} \text{ m}$
Electron transport layer		
Thickness	L^{ETL}	30 nm
Mobility	μ^{ETL}	$1 \times 10^{-6} \text{ m}^2 \text{ V}^{-1} \text{ s}^{-1}$
Relative dielectric constant	ϵ_r^{ETL}	5
Conduction band	E_c^{ETL}	3.9 eV
Valence band	E_v^{ETL}	5.9 eV
Doping density	N_D^+	0 m^{-3}
Hole transport layer		
Thickness	L^{HTL}	10 nm
Mobility	μ^{HTL}	$1.5 \times 10^{-8} \text{ m}^2 \text{ V}^{-1} \text{ s}^{-1}$
Relative dielectric constant	ϵ_r^{HTL}	3.5
Conduction band	E_c^{HTL}	2.5 eV
Valence band	E_v^{HTL}	5.53 eV
Doping density	N_A^-	0 m^{-3}
Generation & Recombination		
Average generation rate	G_{ehp}	$3.4 \times 10^{27} \text{ m}^{-3} \text{ s}^{-1}$
Band-to-band/Bimolecular recombination rate	k_2	$1 \times 10^{-17} \text{ m}^3 \text{ s}^{-1}$
Bulk trap density	N_T	$5 \times 10^{21} \text{ m}^{-3}$
ETL/AL interface trap density	Σ_T^{ETL}	$5 \times 10^{14} \text{ m}^{-2}$
HTL/AL interface trap density	Σ_T^{HTL}	$5 \times 10^{13} \text{ m}^{-2}$
Trap energy level	E_T	4.7 eV
Electron (hole) capture coefficient	$C_{n(p)}$	$1 \times 10^{-14} \text{ m}^3 \text{ s}^{-1}$
Geminate recombination rate	k_f	$1 \times 10^6 \text{ s}^{-1}$
Contact		
Cathode work function	W_L	3.95 eV
Anode work function	W_R	5.48 eV

Table S2: Parameters used in the base case scenario for the OSC.

Parameter	Symbol	Value
Active Layer		
Conduction band	E_c	4.2 eV
Valence band	E_v	5.42 eV
Band gap	E_{gap}	1.22 eV
Effective density of states	N_{cv}	$1.55 \times 10^{26} \text{ m}^{-3}$
Thickness	L	120 nm
Electron mobility	μ_n	$9.32 \times 10^{-8} \text{ m}^{-2} \text{ V}^{-1} \text{ s}^{-1}$
Hole mobility	μ_p	$9.78 \times 10^{-8} \text{ m}^{-2} \text{ V}^{-1} \text{ s}^{-1}$
Relative dielectric constant	ϵ_r	3.5
Initial charge separation distance	a	$1 \times 10^{-9} \text{ m}$
Electron transport layer		
Thickness	L^{ETL}	10 nm
Mobility	μ^{ETL}	$1 \times 10^{-6} \text{ m}^{-2} \text{ V}^{-1} \text{ s}^{-1}$
Relative dielectric constant	ϵ_r^{ETL}	3.5
Conduction band	E_c^{ETL}	4.2 eV
Valence band	E_v^{ETL}	6. eV
Doping density	N_D^+	0 m^{-3}
Hole transport layer		
Thickness	L^{HTL}	40 nm
Mobility	μ^{HTL}	$1 \times 10^{-6} \text{ m}^{-2} \text{ V}^{-1} \text{ s}^{-1}$
Relative dielectric constant	ϵ_r^{HTL}	3.5
Conduction band	E_c^{HTL}	3 eV
Valence band	E_v^{HTL}	5.42 eV
Doping density	N_A^-	0 m^{-3}
Generation & Recombination		
Average generation rate	G_{ehp}	$1.3 \times 10^{28} \text{ m}^{-3} \text{ s}^{-1}$
Band-to-band/Bimolecular recombination rate	k_2	$1.7 \times 10^{-18} \text{ m}^3 \text{ s}^{-1}$
Bulk trap density	N_T	0 m^{-3}
ETL/AL interface trap density	Σ_T^{ETL}	0 m^{-2}
HTL/AL interface trap density	Σ_T^{HTL}	0 m^{-2}
Trap energy level	E_T	4.7 eV
Electron (hole) capture coefficient	$C_{n(p)}$	$1 \times 10^{-13} \text{ m}^3 \text{ s}^{-1}$
Geminate recombination rate	k_f	$1 \times 10^6 \text{ s}^{-1}$
Contact		
Cathode work function	W_L	4.2 eV
Anode work function	W_R	5.42 eV

Influence of parasitic resistances on fill factor and open-circuit voltage

In the following, we derive two criteria to quickly assess whether measurements of the fill factor and open-circuit voltage are influenced by shunt and series resistance. This is especially important when doing such measurements as a function of light intensity.

Shunt resistance

Leakage current will influence the fill factor and open-circuit voltage. This is especially important at low light intensities. Therefore, one needs a solid way of determining whether measurements of FF or V_{OC} are significantly influenced by leakage. In the following, we accept a 1 % deviation. We can set up such a criterion for FF and V_{OC} by considering an equivalent circuit. According to Martin Green's estimate,^[2] the fill factor in the presence of leakage (finite shunt resistance R_{SH}) is given by

$$FF = FF_0 \left(1 - \frac{v_{OC} + 0.7 FF_0}{v_{OC} r_{SH}}\right), \quad (S1)$$

where FF_0 is the fill factor in absence of leakage (the 'real' fill factor), $v_{OC} = \frac{V_{OC}}{nV_{th}}$ is the scaled open-circuit voltage, and $r_{SH} = \frac{R_{SH} J_{SC}}{V_{OC}}$. Typically, $V_{OC} \gg V_{th}$, so the term containing V_{OC} is approximately 1. Also, for good cells, FF is close to 1, so a 1% deviation equals 0.01.¹ This means that FF will be unaffected provided $\frac{FF_0}{R_{SH}} < 0.01$. The shunt resistance may be approximated by

$$R_{SH} \approx \frac{1V}{J_{dark}(-1V)}. \quad (S2)$$

Finally, we find that FF is not significantly affected (less than 1%) if

$$\frac{J_{SC}}{J_{dark}(-1V)} \gtrsim 100. \quad (S3)$$

To illustrate the effect of shunt resistance on FF and how to use the criterion Eq. S3, we use the perovskite reference device (Table S1) and simulate the fill factor as a function of light intensity. Figure S31 demonstrates that Eq. S3 indeed holds. In other words, the fill factor is quite sensitive to leakage current and is impacted unless the light intensity is high enough to ensure that the short-circuit current is much larger than the leakage.

¹Green's formulae are limited to good solar cells anyway.

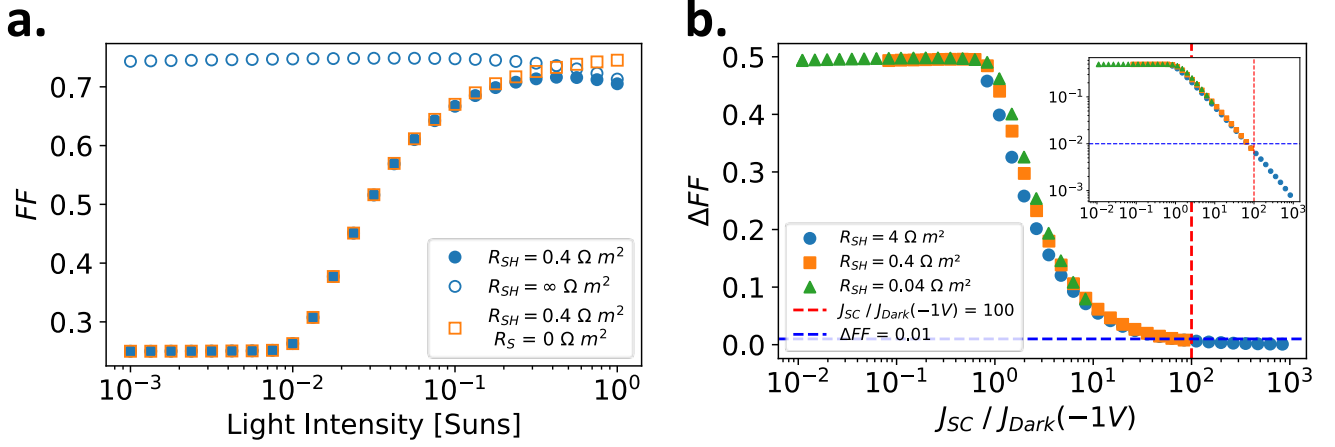


Figure S31: (a) The fill factor of the perovskite base scenario with finite shunt resistance (closed circles) and with infinite shunt resistance (open circles). The effect of removing series resistance is shown by including simulations with zero series resistance (orange rectangles). (b) Shows the deviation of the fill factor as a function of the ratio between the short-circuit current and the leakage current for three different shunt resistances. The dashed red vertical line indicates a ratio of 100 (where the criterion starts to apply) and the blue horizontal line a deviation of the FF of 1 %. The fill factor is thus impacted by leakage unless the ratio is larger than ≈ 100 . The inset depicts the same plot in a log-log scale, where one can see that the fill factor deviates by more than 0.01 if the ratio is smaller than 100.

Now we turn to the open-circuit voltage. We will find that V_{OC} is less affected by shunt resistance, despite the higher bias (and therefore higher leakage current). The current in an equivalent circuit that includes shunt resistance is equal to

$$J(V) = J_{SC} - J_0 \exp\left(\frac{V}{nV_{th}}\right) - \frac{V}{R_{SH}}, \quad (S4)$$

where we have neglected the +1 term in the exponential. At open-circuit the current density is zero and we have

$$J_{SC} - \frac{V}{R_{SH}} = J_0 \exp\left(\frac{V}{nV_{th}}\right) \quad (S5)$$

If we use the normal result for V_{OC} in the absence of parasitic resistances, and replace J_{SC} by $J_{SC} - \frac{V_{OC}}{R_{SH}}$, we have

$$V_{OC} \approx nV_{th} \ln\left(\frac{J_{SC} - 1/R_{SH}}{J_0}\right). \quad (S6)$$

The deviation of V_{OC} due to leakage current is given by

$$\Delta V_{OC} = nV_{th} \left\{ \ln J_{SC} - \ln\left(J_{SC} - \frac{1}{R_{SH}}\right) \right\}. \quad (S7)$$

Using a first order Taylor series yields

$$\Delta V_{OC} = nV_{th} \frac{J_{dark}(-1V)}{J_{SC}}. \quad (S8)$$

Now we require ΔV_{OC} be smaller than 0.01 V (i.e. 1%) and obtain

$$\frac{J_{SC}}{J_{dark}(-1V)} \gtrsim 100nV_{th}, \quad (S9)$$

which is very similar to Eq. S3, the only difference being the nV_{th} term. At room temperature and for $n \approx 2$, we have

$$\frac{J_{SC}}{J_{dark}(-1V)} \gtrsim 5, \quad (S10)$$

which shows that the open-circuit voltage is indeed less sensitive to leakage. In other words, measurements of V_{OC} versus light intensity will be correct down to lower intensities than similar measurements of FF . Figure S32 shows the influence of leakage on the open-circuit voltage. Indeed, if the criterion (Eq. S9) is satisfied, the deviation in open-circuit is below 0.01 V.

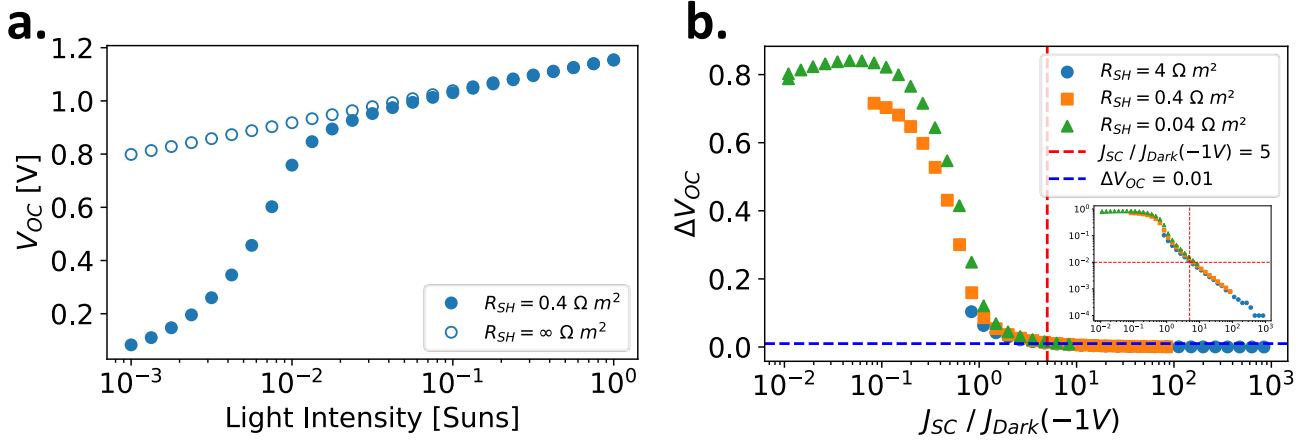


Figure S32: (a) Open-circuit voltage of the perovskite base scenario with finite shunt resistance (closed symbols) and with infinite shunt resistance (open symbols). (b) Shows the deviation of the open-circuit voltage as a function of the ratio between the short-circuit current and the leakage current for three different shunt resistances. The dashed red vertical line indicates a ratio of 5 (where the criteria starts to apply) and the blue horizontal line a deviation of the V_{OC} of 0.01. The inset depicts the same plot in a log-log scale, where one can see that the open-circuit voltage deviates by more than 0.01 V if the ratio is smaller than 5 (see Eq. S10).

Series resistance

If there is a noticeable amount of series resistance in the equivalent circuit of the device, then this will impact the fill factor. The short-circuit current density will only change, if the series resistance is very high. The open-circuit voltage is not impacted by series resistance as there is no flow of current and, hence, no change in voltage. Therefore, we limit our discussion to mild series resistance only, i.e. the case where FF changes, but the short-circuit current does not. In order to derive how FF changes by series resistance, we assume that the strongest effect on the maximum power point is in the shift of its voltage (V_{MPP}), whereas its current (J_{MPP}) is assumed to be unaffected. Then, we can write FF as

$$FF = \frac{J_{MPP}(V_{MPP} - J_{MPP}R_s)}{(J_{SC}V_{OC})}. \quad (\text{S11})$$

The change in FF , ΔFF is then equal to

$$\Delta FF = \frac{J_{SC}R_s}{V_{OC}}, \quad (\text{S12})$$

where we have approximated J_{SC} by J_{MPP} . As J_{MPP} is smaller than J_{SC} , Eq. S12 overestimates the change in FF . If we, again, accept an error of 0.01, then we have the criterion that FF is valid is

$$J_{SC} < \frac{0.01V_{OC}}{R_s}. \quad (\text{S13})$$

Alternatively, if we take $V_{OC} \approx 1\text{V}$, then we have that

$$J_{SC}R_s < 0.01\text{V}. \quad (\text{S14})$$

Figure S31 shows the impact of series resistance on the fill factor.